



Structural evolution of sheared margin basins: the role of strain partitioning. Sørvestsnaget Basin, Norwegian Barents Sea

Thomas B. Kristensen,*  Atle Rotevatn,* Maria Marvik,* Gijs A. Henstra,* Robert L. Gawthorpe*  and Rodmar Ravnås†

*Department of Earth Science, University of Bergen, Bergen, Norway

†A/S Norske Shell, Tananger, Norway

ABSTRACT

Spatio-temporal analysis of basins formed along sheared margins has received much less attention than those formed along orthogonally extended margins. Knowledge about the structural evolution of such basins is important for petroleum exploration but there has been a lack of studies that document these based on 3D seismic reflection data. In this study, we demonstrate how partitioning of strain during deformation of the central and southern part of the Sørvestsnaget Basin along the Senja Shear Margin, Norwegian Barents Sea, facilitated coeval shortening and extension. This is achieved through quantitative analysis of syn-kinematic growth strata using 3D seismic data. Our results show that during Cenozoic extensional faulting, folds and thrusts developed coevally and orthogonal to sub-orthogonal to normal faults. We attribute this strain partitioning to be a result of the right-lateral oblique plate motions along the margin. Rotation of fold hinge-lines and indications of hinge-parallel extension indicate that the dominating deformation mechanism in the central and southern Sørvestsnaget Basin during opening along the Senja Shear Margin was transtensional. We also argue that interpretation of shortening structures attributed to inversion along the margin should consider that partitioning of strain may result in shortening structures that are coeval with extensional faults and not a result of a separate compressional phase.

INTRODUCTION

The structural evolution of basins at orthogonally extended rifts and passive margins is well documented from the study of outcrop and subsurface studies (e.g. the Corinth Rift, Bell *et al.*, 2009; the East African Rift, Ebinger, 1989; the Suez Rift, Moustafa, 1993; Sharp *et al.*, 2000; the North Sea Rift, Badley *et al.*, 1988; Ziegler, 1992; the Atlantic margins of North America, Withjack *et al.*, 1998; Africa, Lehner & De Ruiter, 1977; Spathopoulos, 1996; the offshore Suez Gulf; Sharp *et al.*, 2000; Jackson & Rotevatn, 2013) as well as numerical and physical analogue modelling (e.g. Huismans *et al.*, 2001; McClay *et al.*, 2002; Corti *et al.*, 2003; Naliboff & Buitert, 2015). Less attention has been focused on natural examples of basins developed along sheared margins (i.e. margins dominated by strike-slip tectonics), where most work have focused on margin-scale structure (e.g. Jackson *et al.*, 1990; Faleide *et al.*, 1991; Clift *et al.*, 1997; Mjelde *et al.*, 2002), regional evolution (e.g. Faleide *et al.*, 1993a;

Doré *et al.*, 2015) or physical experiments (e.g. Scrutton, 1979; Lorenzo, 1997; Vågenes, 1997; Basile & Brun, 1999).

A staged evolution of sheared margins was proposed by Bird (2001): (i) shearing of continental crust and complex rifting; (ii) development of an active transform boundary separating oceanic and continental crust; (iii) passive margin formation along an inactive fracture zone that also separates oceanic and continental crust. Bird (2001) stated that sheared margin evolution typically involves continental rifting and intensely deformed rift sequences over rotated basement blocks. Thermal uplift due to heat transfer as the seafloor spreading axis moves along the margin is expected to produce a ridge that traps sediments. When the ridge has passed the margin it is characterized by normal tectonic and thermal subsidence. Fault styles and physiography that can be expected at continental transforms and major strike-slip faults are summarized by Kearey & Vine (1996); (i) linear fault scarps and laterally offset surface features, (ii) step overs, push-ups and pull-apart basins, (iii) releasing and restraining bends, (iv) strike slip duplexes, fans and flower structures, (v) strike-slip partitioning in transpression and transtension.

Correspondence: Thomas B. Kristensen, Department of Earth Science, University of Bergen, PB 7803, N-5020 Bergen, Norway. E-mail: Thomas.Kristensen@uib.no

The latter point relating to strain partitioning is central, since the importance of strain partitioning is well known from strike-slip dominated systems (e.g. Christie-Blick & Biddle, 1985). Sanderson & Marchini (1984) explained how strain can be partitioned into shortening and extension during simple shear, transtension (e.g. Dewey *et al.*, 1998; Oldow, 2003; De Paola *et al.*, 2005) and transpression (e.g. Dewey *et al.*, 1998; Holdsworth *et al.*, 2002; Jones *et al.*, 2004; Clegg & Holdsworth, 2005). Notably, Dewey *et al.* (1998) demonstrated that partitioning of non-coaxial strike-slip and coaxial strains is a characteristic feature for many transpression and transtension zones, especially if the far-field plate displacement direction is markedly oblique (e.g. $<20^\circ$) to the plate or deformation zone boundary.

Strain partitioning is also recorded in many obliquely extending plate boundaries, i.e. transitional margins that fall between rifted margins (dominated by orthogonal extension) and sheared margins (dominated by strike-slip motion), so-called rift-shear margins (e.g. Seiler *et al.*, 2010). One such example is the Gulf of California where oblique divergence is accommodated by strike-slip and normal faulting, low-angle detachment faulting and folding (e.g. Seiler *et al.*, 2010; Fossen *et al.*, 2013). Strain partitioning is also common in oblique convergence settings, such as along the San Andreas Transpression System, where simple shear is accommodated by strike-slip faults and the convergent pure shear component is accommodated by folding (Mount & Suppe, 1987).

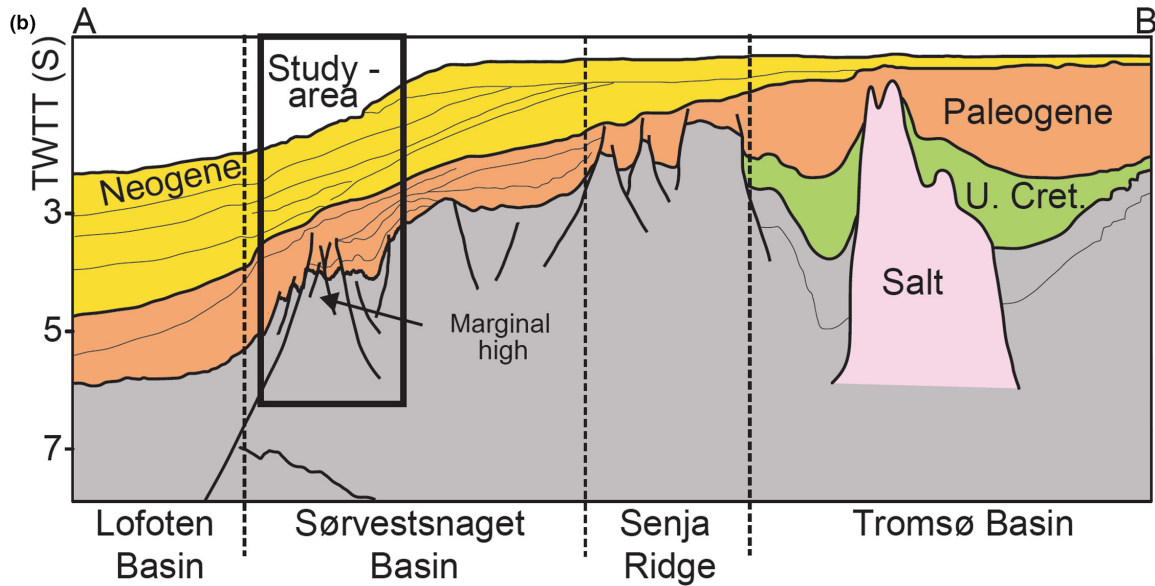
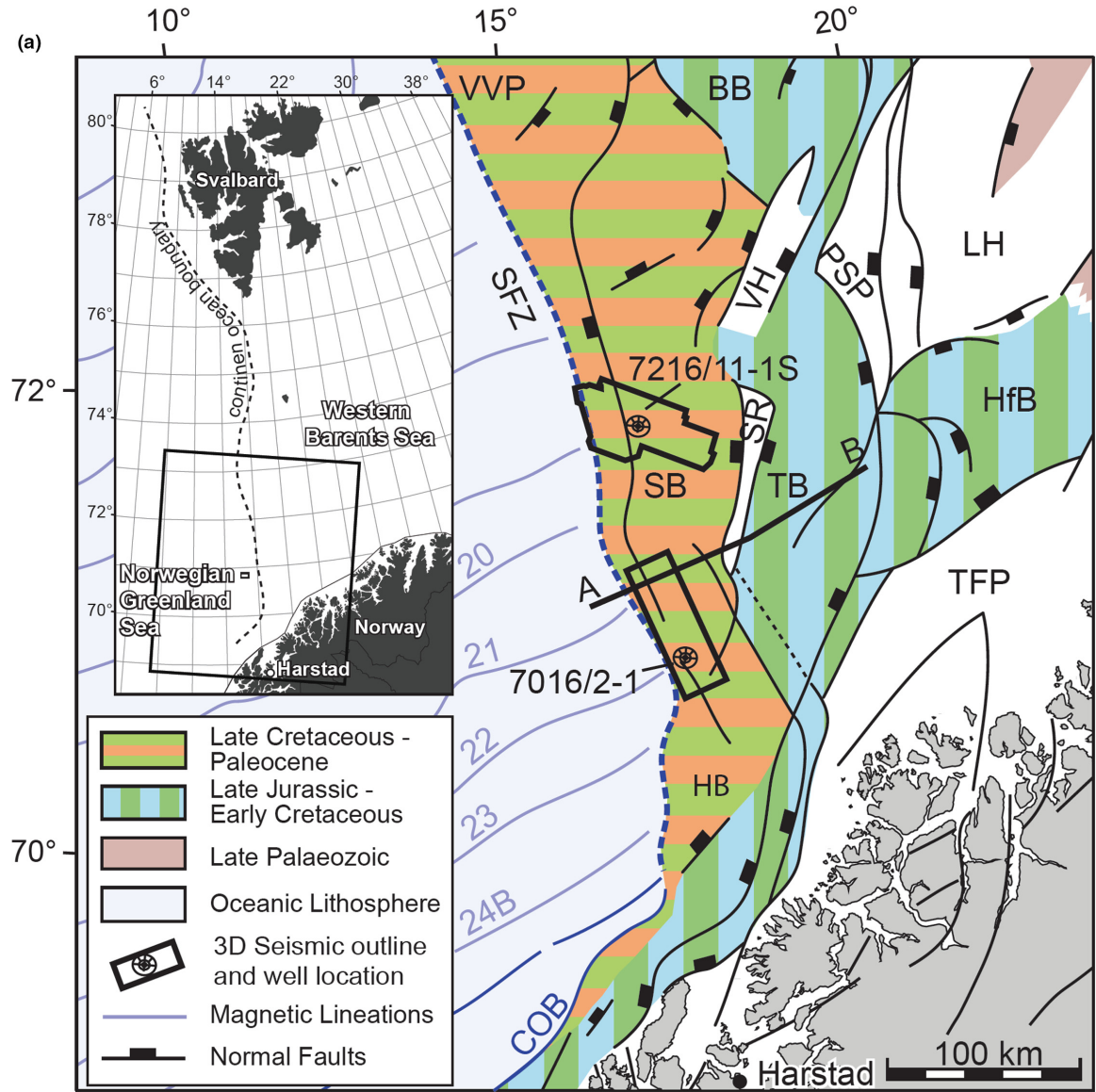
Despite the general knowledge of sheared margins, the structural style and evolution of sedimentary basins at such margins remains under-researched. In this study, we analyse the sheared western Barents Sea margin, offshore northern Norway, focusing on the Sørvestsnaget Basin (e.g. Ryseth *et al.*, 2003; Faleide *et al.*, 2008; Fig. 1). Despite the fact that it is well established that the Senja Shear Margin was exposed to oblique divergence in the Eocene (e.g. Reksnes & Vågnes, 1985; Eldholm *et al.*, 1987), there are no previous studies, to our knowledge, that discuss the details of how regional strains were accommodated, or, more specifically, partitioned, during the formation and deformation of basins along the margin. Three-dimensional reflection seismic and wellbore data allow us to quantitatively analyse the structural evolution of this sheared margin basin and elucidate the role of strain partitioning in the development of such basins.

GEOLOGICAL SETTING

The western Barents Sea is part of the continental shelf of north-western Eurasia, located north of Norway and bordered by the Norwegian–Greenland Sea and the Svalbard Archipelago in the west (inset map in Fig. 1a). The western Barents Margin includes the continental margin from Svalbard in the north to the Norwegian mainland in the south, a distance of about 1000 km (Faleide *et al.*, 1996; Fig. 1). The margin evolution and the spreading history of the Norwegian Greenland Sea is well established on a regional and plate tectonic scale through several studies (e.g. Talwani & Eldholm, 1977; Eldholm *et al.*, 1987; Faleide *et al.*, 1984, 1991, 1996, 2008; Gabrielsen, 1984; Gudlaugsson *et al.*, 1998; Tsikalas *et al.*, 2002). The western Barents Sea include basins formed during different phases of regional tectonism that affected the North Atlantic region in Palaeozoic to Cenozoic times (e.g. Faleide *et al.*, 1993a,b). These were the result of a series of rift events that followed in the wake of the Ordovician to Devonian Caledonian Orogeny, whose structural imprint influenced the post-Caledonian evolution of the Barents Sea (Doré, 1991). This protracted phase of several rift events in the North Atlantic region culminated with continental breakup, opening of the Norwegian–Greenland Sea, and the separation of Eurasia and Greenland in the Early Cenozoic (Doré, 1991; Faleide *et al.*, 1993a,b; Ritzmann & Faleide, 2007). In the western Barents Sea, the most significant of these regional rift events were those that occurred in i) Late Palaeozoic, ii) Middle/Late Jurassic–Early Cretaceous and iii) Late Cretaceous–Palaeogene.

In the Late Cretaceous to middle Palaeogene, the extension between Norway and Greenland was accommodated by transcurrent movement and deformation within the De Geer Zone, which was a precursor for the present-day western Barents Sea–Svalbard margin (marked as the continent ocean boundary in the inset map in Fig. 1a) (Eldholm *et al.*, 1987, 2002; Faleide *et al.*, 1988, 1993a,b, 2008; Breivik *et al.*, 1998). The Senja Fracture Zone was a part of the De Geer Zone, a mega-shear system linking the North Atlantic to the Arctic prior to breakup (Eldholm *et al.*, 2002). The De Geer Zone megashear system was the precursor for the development of the western Barents Sea – Svalbard margin which consists of two large shear segments and a central rifted segment (Myhre *et al.*,

Fig. 1. (a) Regional map (based on Faleide *et al.*, 2010) indicating location of major basins and highs in the Western Barents Sea as well as position of the two available 3D seismic datasets that delineate the study area. Numbering of magnetic anomalies is based on Talwani & Eldholm (1977) and Tsikalas *et al.* (2001). Annotations on top map: BB (Bear Island), COB (Continent Ocean Boundary), HB (Harstad Basin), HfB (Hammerfest Basin), LH (Loppa High), PSP (Polheim Sub Platform), SB (Sørvestsnaget Basin), SFZ (Senja Fracture Zone), SR (Senja Ridge), TB (Troms Basin), TFP (Troms Finnmark Platform), VH (Veslemøy High), VVP (Vestbakken Volcanic Province). (b) Regional 2D seismic line (location in top map; A–B) displaying the study area in relation to the surrounding major basins and highs. Grey colouring represent strata or basement without well-control.



1982; Eldholm *et al.*, 1987; Faleide *et al.*, 1988, 2008). The Senja Fracture Zone (marked SFZ in Fig. 1a) is the southernmost of these segments and developed during the Eocene opening of the Norwegian–Greenland Sea, first by continent–continent shear between the Laurentia and Baltica plates followed by continent ocean shear and quiescence since the earliest Oligocene (Faleide *et al.*, 2008).

The Sørvestsnaget Basin is delineated to the west by the Senja Fracture Zone and is characterized as a deep Cretaceous and Cenozoic basin (approx. location: 71°–73°N, 15°–18°E) (Gabrielsen *et al.*, 1990; Ryseth *et al.*, 2003). The pre-Tertiary evolution of the Sørvestsnaget is not well established but Breivik *et al.* (1998) stated that the thick late Cretaceous (~6 km thickness) interval may be related to a phase of Late Cretaceous rifting climaxing in Cenomanian and Middle Turonian as recorded on the conjugate east coast of Greenland. The central and northern parts of the Sørvestsnaget basin formed a pull-apart basin in Late Cretaceous–Early Palaeocene and a relatively complete Palaeocene succession was deposited under deep marine conditions (Ryseth *et al.*, 2003). The deep marine conditions continued throughout the Eocene with deposition of significant sandy submarine fans during the Middle Eocene. Middle-late Eocene active salt diapirism in the Sørvestsnaget Basin was coeval to the opening of the Norwegian–Greenland Sea (Perez-Garcia *et al.*, 2013). Coeval to the shear along the Senja Fracture Zone and basin formation in the Sørvestsnaget Basin transpression along the Hornsund Fault Zone led to orogenesis along the western part of Svalbard (inset map in Fig. 1a) creating the W Spitsbergen Fold Belt. The orogenesis along western Svalbard led to Palaeocene–Eocene basin formation in the Spitsbergen Central Basin (Nøttvedt *et al.*, 1988). The Svalbard Fold and Thrust Belt orogenesis is characterized by a partitioning of strain between strike slip faults and broad zones of convergent strain during overall transpression (e.g. Leever *et al.*, 2011).

During the earliest Oligocene the relative plate motion changed and shear along the Western Barents Margin was followed by east–west oriented extension seen as a series of NNW–SSE trending normal faults (Eldholm *et al.*, 2002). Uplift and burial of the margin by a thick clastic wedge is characteristic of the late Cenozoic evolution (Faleide *et al.*, 2008). Erosion estimates of the Palaeogene sequence range from 1000 to 1500 m in the southwestern Barents Sea (Faleide *et al.*, 1993a,b).

DATA AND METHODS

For this study, two 3D seismic reflection surveys are used. The southernmost MC3D_TRIII08 survey, henceforth referred to as the southern survey covers c.

1500 km² and was acquired in 2008, whereas the northernmost NH9803 survey, henceforth referred to as the northern survey, covers c. 2000 km² (Figs 1 and 2a) and was acquired in 1998. Both surveys consist of pre-stack time migrated data. The southern survey has an inline spacing of 25 m and a crossline spacing of 12.5 m; inlines are oriented NNW–SSE, parallel to the strike of the sheared margin. The northern survey has an inline spacing of 37.5 m and a crossline spacing of 12.5 m; inlines are oriented NW–SE, also parallel to the strike of the sheared margin. Velocity models were produced for both 3D surveys to allow for depth conversion of the interpreted horizons. Both velocity models are based on seismic stacking velocities from 2D seismic reflection data using a Dix conversion and a 5% reduction to account for overestimating the seismic velocities. Fig. 2 shows the velocity model and seismic section in time (Fig. 2a) as well as depth-converted sections in both 1:4 (Fig. 2b) and 1:1 scale (Fig. 2c). The table in Fig. 2b shows the accuracy of the depth conversion by comparing the depth from seabed to three selected reflections in both the well and the depth converted section (e.g. 37 m mismatch for reflection Rc). Well 7016/2-1(T2) located within the southern survey and well 7216/11-1S located within the northern survey (Fig. 1) provide calibration of the age of the mapped horizons and the lithology of the investigated intervals (Fig. 3). Key-mapped horizons in the study area are furthermore tied to the stratigraphy of the Tromsø Basin using 2D reflection seismic lines (Fig. 1). Seven horizons were interpreted based on continuity and quality of the seismic reflectivity and were tied to the wells. Age control for the southern survey is based on biostratigraphy from well 7016/2-1(T2), whereas for the northern survey the age of the interpreted horizons are based on Ryseth *et al.* (2003) and their interpretation of well 7216/11-1S. Direct correlation of the horizons between the two surveys was not possible due to lack of seismic data coverage and the correlation is thus based on the seismic character and the age constraints from well data.

Fault activity exerts a primary control on accommodation generation in rift basins (Ravnås & Steel, 1997) and in this study, we apply both qualitative and quantitative methods for kinematic fault and fold analysis. Qualitative fault analysis included cross-sectional observation of changes in stratigraphic thickness and architecture of syn-tectonic, growth strata, coupled with isopach maps to identify fault and fold-controlled depocentres. Quantitative methods such as throw distribution analysis are used in combination with stratigraphic thickness variations to constrain the temporal and spatial evolution of normal faults (e.g. Petersen *et al.*, 1992; Childs *et al.*, 1995; Huggins *et al.*, 1995; Mansfield & Cartwright, 1996; Walsh *et al.*, 2002, 2003; Baudon & Cartwright, 2008a,b,c; Giba *et al.*, 2012; Jackson & Rotevatn, 2013; Tvedt *et al.*, 2013, 2016; Jackson *et al.*, 2017). Throw rather than true

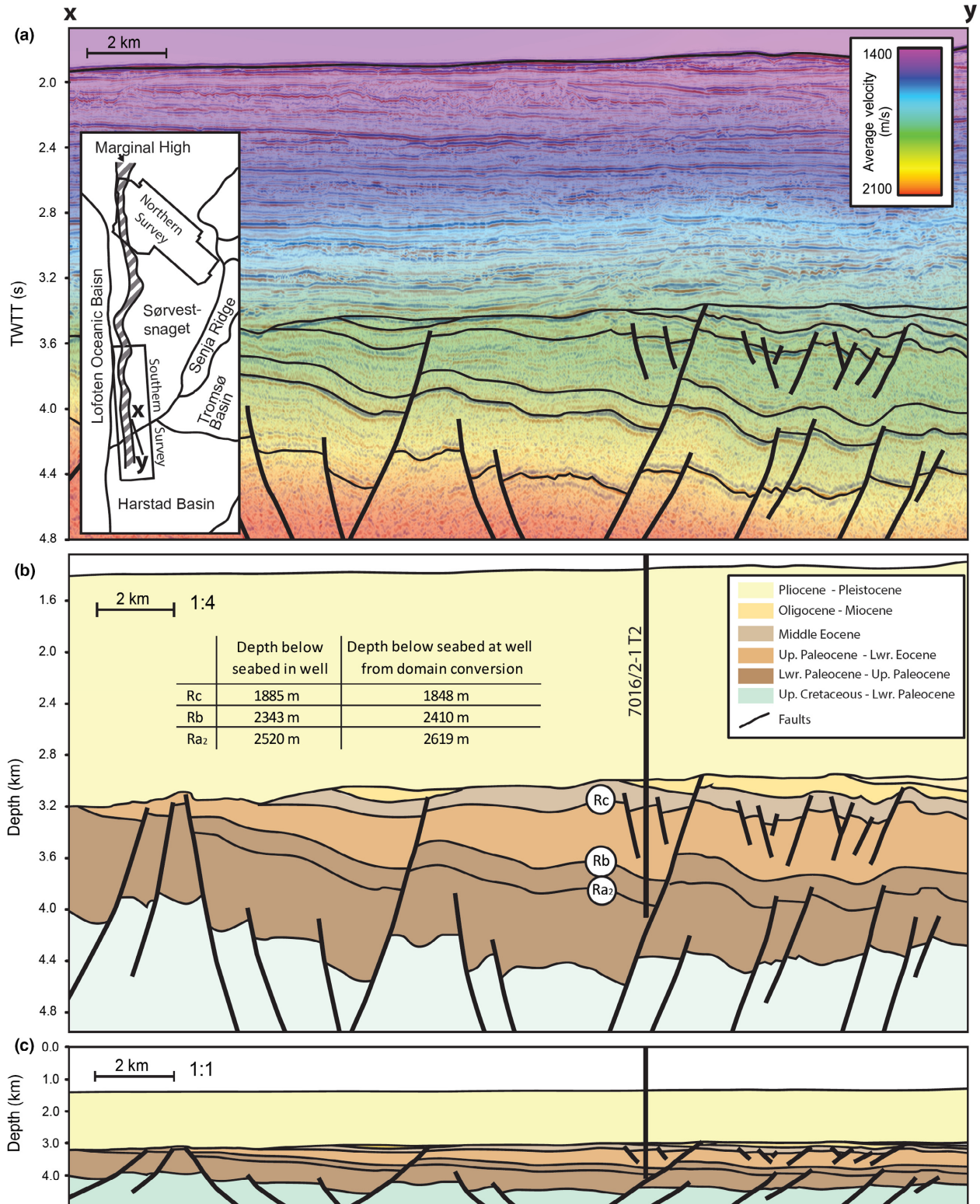


Fig. 2. (a) Seismic section overlaid by the velocity model, the velocity model was constructed using stacking velocities from 2D data. Location of seismic section is marked x-y in the inset structural element map which shows the study area location with respect to the major basins of the Southwestern Barents Sea. Note that the marginal high, which is also named the Senja Fracture Zone, is present in both areas. (b) 1:4 scale (vertically exaggerated) depth-converted version of the same section as in (a). The table shows the difference in depth from the seabed to selected reflections in the well and in the depth-converted section. (c) Same section as in (a) and (b) but in 1:1 scale (no vertical exaggeration).

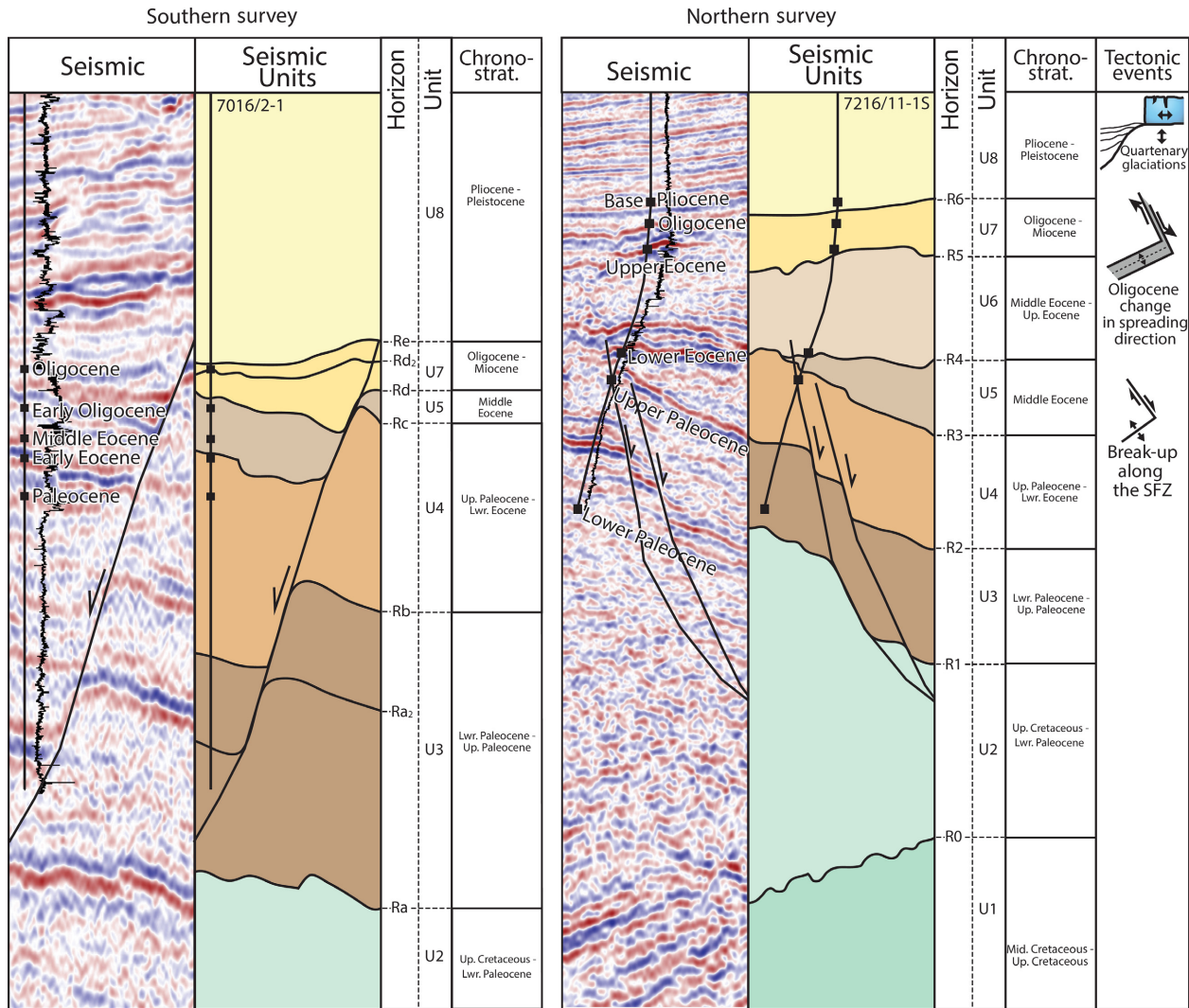


Fig. 3. Seismic stratigraphy and well-tie for both 3D surveys (southern survey and northern survey). The well is displayed together with well-tops and gamma ray logs. The tectonic events are based on the evolution of the south-western Barents Sea described in Faleide *et al.* (1993a).

displacement is used to establish control on fault offset due to a lack of displacement vector indicators in the seismic data. The seismic resolution allowed for confident throw mapping, however, footwall and hanging-wall cut-offs were extrapolated in places with fault drag (*sensu* Wilson *et al.*, 2013). Mapping of throw variations requires that the sedimentation rate was equal to or higher than the separation rate during fault activity (overfilled or balanced basins) so that the complete growth history of the faults is recorded by syn-rift sediments (e.g. Childs *et al.*, 2003). Throw-depth (T-z) plots are produced at selected locations with a fixed spacing along the studied faults to elucidate throw variations potentially related to dip linkage (e.g. Mansfield & Cartwright, 1996; Tvedt *et al.*, 2013), syn-sedimentary faulting (high throw gradients due to fault growth being restricted by the depositional surface) and blind fault propagation (e.g. Nicol

et al., 1996; Tvedt *et al.*, 2013). Throw values are calculated using depth-converted horizons and are plotted at the mid-point between hangingwall and footwall cut-offs (e.g. Rykkelid & Fossen, 2002; Baudon & Cartwright, 2008b; Jackson & Rotevatn, 2013; Tvedt *et al.*, 2013). Variations in stratigraphic thickness across faults are analysed by the use of isochore thickness maps and expansion indices (EI). The expansion index is the ratio of hanging-wall vs. footwall thickness of a specific stratigraphic interval and is calculated using depth-converted horizons. This provides a dimensionless value where an expansion index of 1 indicates no change in thickness across the fault, whereas values >1 may indicate fault growth (e.g. Thorsen, 1963; Cartwright *et al.*, 1998; Bouroulllec *et al.*, 2004; Jackson & Rotevatn, 2013; Tvedt *et al.*, 2013). As for faults the onset and duration of folding are quantified by analysing growth packages (e.g. Suppe *et al.*, 1992;

Storti & Poblet, 1997; Higgins *et al.*, 2009). The ratio of flank and crest stratigraphic thickness was measured for folds (*sensu* Higgins *et al.*, 2009) to quantify syn-tectonic growth. This assumes that the variation in layer thickness is due to syn-tectonic sedimentation where pre-kinematic layers should have a constant cross-fold thickness, whereas the syn-tectonic layers should thin towards and atop a fold (Higgins *et al.*, 2009).

SEISMIC STRATIGRAPHY OF THE SOUTHERN SØRVESTSNAGET BASIN

Eight seismic stratigraphic units bounded by key seismic horizons form the foundation of our analyses (Fig. 3). The seismic units are numbered U1 through U8 within the northern survey, in the southern survey only six of these units are present (Fig. 3). These units cover stratigraphy from middle Cretaceous to Pleistocene. The seismic units were based on seismic horizons named R0 through R6 in the southern survey, and Ra through Re in the northern survey. For the southern survey U3 and U7 have internal reflections that are interpreted and included in the study as Ra₂ and Rd₂ respectively (Fig. 3). Wells 7016/2-1(T2) and 7216/11-1S provide calibration of the age of the mapped seismic horizons. The seismic stratigraphy was further calibrated with that of Ryseth *et al.* (2003), based on seismic stratigraphic similarities and we adopt their stratigraphic colour scheme (Fig. 3). A confident 2D seismic tie between the two 3D seismic surveys was not available; however, based on comparison of the general seismic signature and reflection characteristics, the seismic horizons and units in the two 3D seismic surveys are qualitatively determined to be equivalent. This is except for U1 and U6 in the southern survey due to the absence of any continuous strong reflections equivalent to the R1 reflection in the northern survey, as well as for unit U6 due to lack of middle-late Eocene strata in the 7016/2-1 well (Fig. 3).

The middle Cretaceous to upper Cretaceous interval has not been penetrated by the wells in this study. We follow Ryseth *et al.* (2003) who argue that the Cretaceous–Cenozoic boundary is likely present just beneath well 7216/11-1S. This implies that U1 in the northern survey consists of middle to upper Cretaceous strata. Accordingly, we attribute U2 to cover upper Cretaceous to lower Palaeocene strata. The intervals of interest comprise the Palaeogene and Lower Neogene succession in the basin (seismic units U3 to U7; Fig. 3). Seismic unit U3 comprise lower to upper Palaeocene strata, whereas U4 consist of a transition from upper Palaeocene to lowermost Eocene strata. In the northern survey, both U5 and U6 cover the Eocene interval, with U5 comprising the middle Eocene, and U6 the middle to upper Eocene. Within the southern survey, seismic unit U5 is interpreted to cover

lower to middle Eocene strata. The Oligocene to Miocene interval is covered by U7, whereas U8 covers the entire stratigraphic interval of Pliocene and Pleistocene age strata. The Pliocene–Pleistocene sequence is thought to postdate the deformation phase of interest in this study and is by Faleide *et al.* (1993a,b) described as a post-Oligocene wedge related to uplift and erosion to the east, in the greater Barents Sea, shedding large amounts of sediments into the oceanic Lofoten Basin.

STRUCTURAL ANALYSIS

The study area is characterized by numerous normal faults, reverse faults and folds (Figs 4, 5 and 6). To the west the study area is bounded by an N-S striking marginal high, which constitutes the Senja Fracture Zone that is evident on both 3D seismic surveys (Figs 4, and 6). This marginal high is bounded by several segmented fault strands that are generally W-dipping and oriented N-S. In some areas the cross-sectional expression of the marginal high is that of a single fault strand, whereas in other areas throw is distributed across a series of down-stepping fault terraces (e.g. Figs 4 and 6). Eastward of the marginal high the basin is characterized by a combination of extensional (normal faults) and contractional structures (folds and thrusts) that strike orthogonal to sub-orthogonal to one another (Figs 4, 5 and 6). All the structures are oriented obliquely to the strike of the marginal high, where the extensional structures are chiefly normal faults with variable throw oriented NE-SW. The contractional structures are oriented mainly NW-SE and include gentle to open folds and thrust faults (Figs 4 and 6). Figure 5 displays a 3D-view of the geometric relationship between NW dipping normal faults and NW-SE striking folds and reverse faults. The northern survey reveals a salt diapir located in the SE part of the survey which previously has been described by Perez-Garcia *et al.* (2013).

Extensional structures

Extension-related structures include arrays of predominantly NW dipping normal faults with smaller SE-dipping antithetic faults (Figs 4 and 6). The strike of these faults is oblique to that of the marginal high (approximately 34–43°). The larger faults have throw maxima of up to 220 ms TWTT (c. 370 m), and lengths up to 10 km in the southern survey and up to 900 ms TWTT (c. 1220 m) throw and lengths of up to 22 km in the northern survey.

All the larger faults have a broadly linear expression and many of the minor faults appear to be isolated, whereas the larger faults show a segmented nature with splays, relays and breached relays (Figs 4 and 5). The extensional faults occur throughout the study area and in

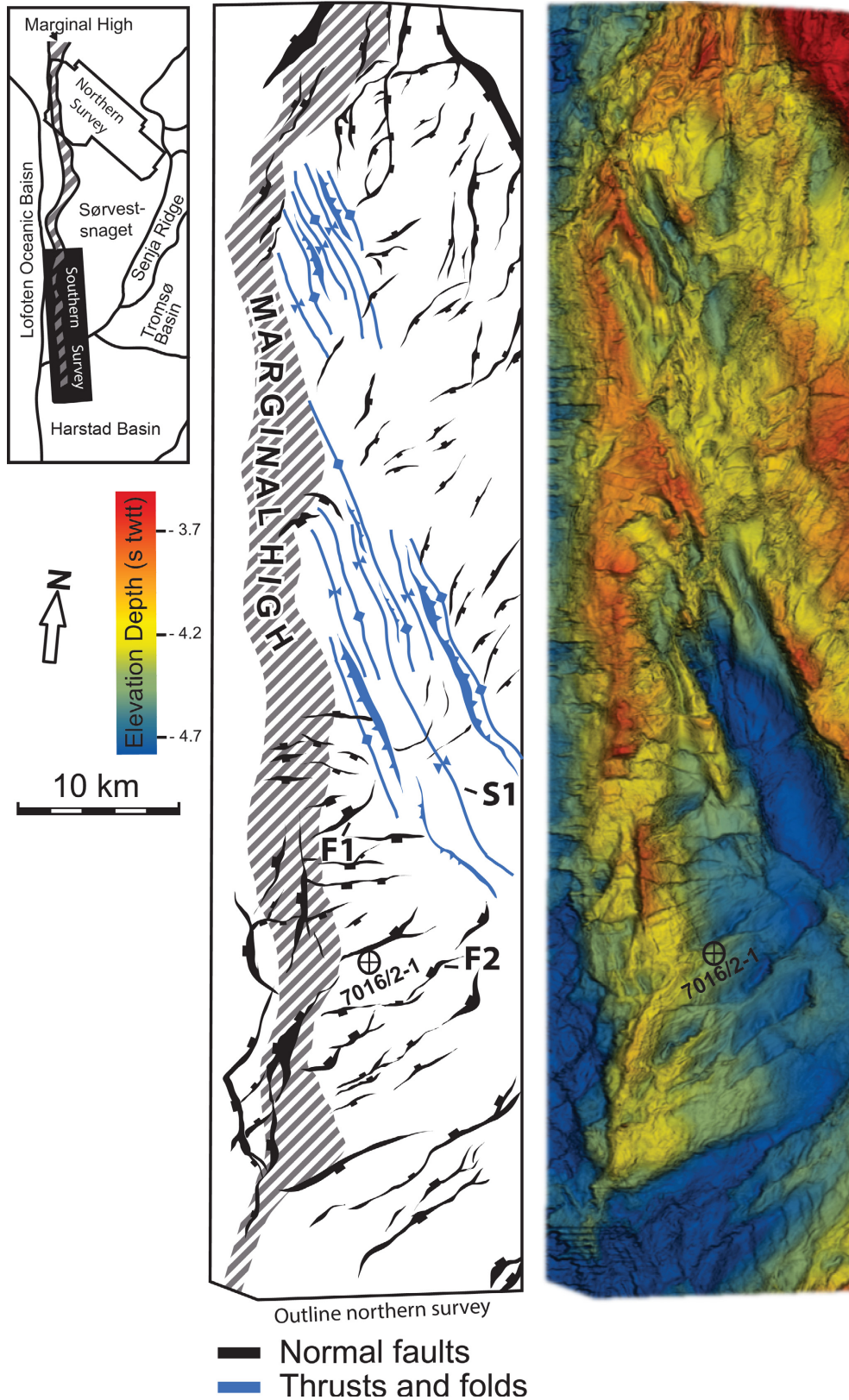


Fig. 4. Structural map and map (in time, seconds twtt) of base lower – upper Palaeocene reflection (Ra) in the southern survey including approximate location of well 7016/2-1 (note that the well does not penetrate to this depth, see e.g. Fig. 2). The location of the marginal high is marked by a grey hatched area. Faults F1 and F2 as well as syncline S1 are annotated.

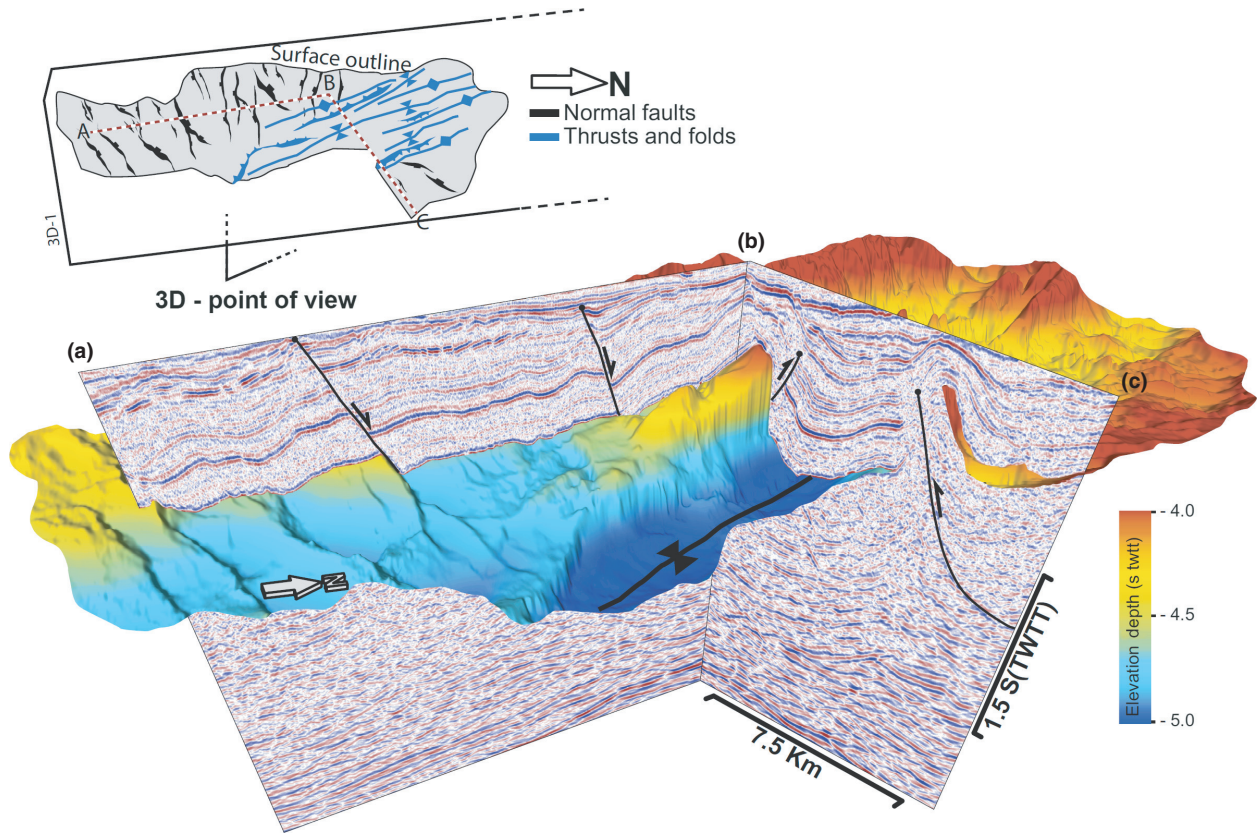


Fig. 5. 3D oblique view of opposing structural elements displaying normal faults dipping towards NNW along a-b and folds and reverse faults striking NW-SE along b-c.

cross-sectional view, most faults tip out upwards in the Oligocene to Miocene unit (U7), whereas some minor faults tip out upwards at deeper levels (e.g. faults tipping out in lower to upper Palaeocene, U3; Fig. 7). The lower parts of the faults are poorly imaged and their downdip termination is therefore not possible to resolve.

Four representative faults (faults F1–F4, Figs 7 and 8) are analysed. For the southern survey the plots in Fig. 7 display the throw variation with depth for faults F1 and F2, and in the northern survey for faults F3 and F4 in Fig. 8. All faults record a throw maximum at the top reflection for Unit 2 (Ra and R1 reflections), except for F1 which have a throw maximum at the top reflection of Unit 3 (Rb reflection) (Figs 7 and 8). The throw gradients of faults F1, F2, F3 and F4 exhibit a marked increase in throw gradient upwards from the Rb, Rc, R3 and R2 horizons respectively (T_g = throw gradient in Figs 7 and 8). Upward from top U5 the throw gradient is low for F3 and F4, however, they also show a high throw gradient for U7. Fault F1 appears to tip out in the Oligocene–Miocene unit (U7); however, in this location the fault is close to the marginal high and the upwards tip-out of the fault is down-lapped by Pliocene reflections (U8) (Fig. 7).

Stratigraphic thickness variations

The studied interval is separated into units displaying fault-ward hanging-wall thickening and units that exhibit uniform thickness across faults. This is recorded and quantified by expansion indices (Figs 7 and 8) and isochore thickness maps (Fig. 9). Hanging-wall thickening of upper Palaeocene to middle Eocene strata is evident on thickness maps for the southern survey (U4 and U5; Fig. 9a, c) and the northern survey (U4 and U5; Fig. 9b, d) respectively. A shift in the southern survey from marked fault-controlled depocentres in the upper Palaeocene–lower Eocene unit (U4) to less defined fault-control in the middle Eocene unit (U5) is evident in Fig. 9a, c. In the northern survey there is a clear shift from distributed fault-controlled hanging-wall thickening in the upper Palaeocene to lower Eocene unit (U4) to a localization of hanging-wall expansion at F4 in the middle Eocene unit (U5) in Fig. 9b, c. The marked hanging-wall expansion is confirmed by expansion indices for fault F1 and F2 in the southern survey (Fig. 7) where a maximum hanging-wall expansion is apparent in upper Palaeocene to lower Eocene strata with expansion index values between 1.9

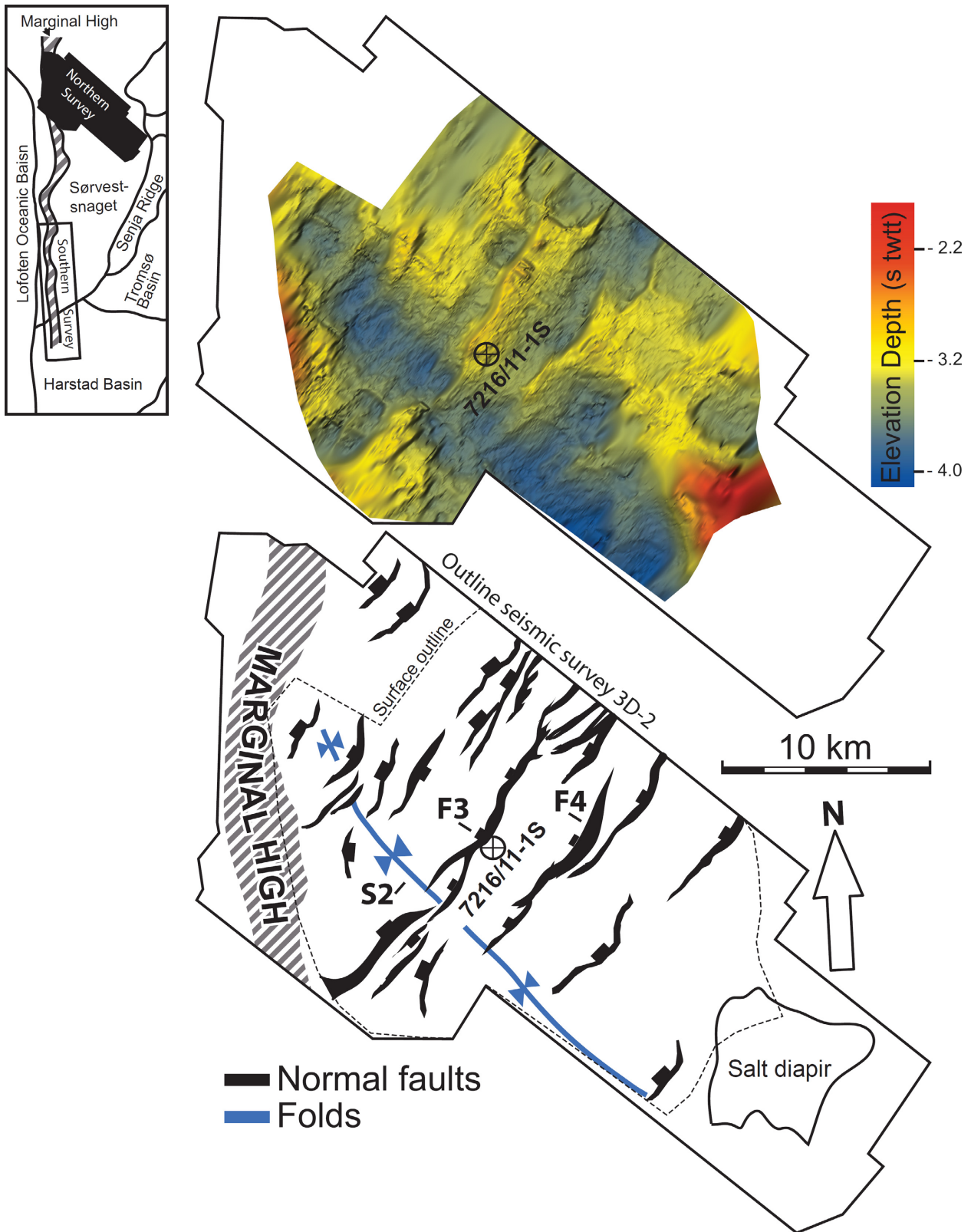


Fig. 6. Structural map (in time, seconds twtt) of base upper Palaeocene–lower Eocene (R3) in the northern survey. The extent of the map towards east is limited by correlation of reflections across large offset faults in the marginal high, to SE by a large salt diapir (approx. areal extent of the diapir is shown) and to the NW by poor seismic quality. The approximate location of the marginal high is marked by a grey hatched area. Faults F3, F4 and syncline S2 are annotated.

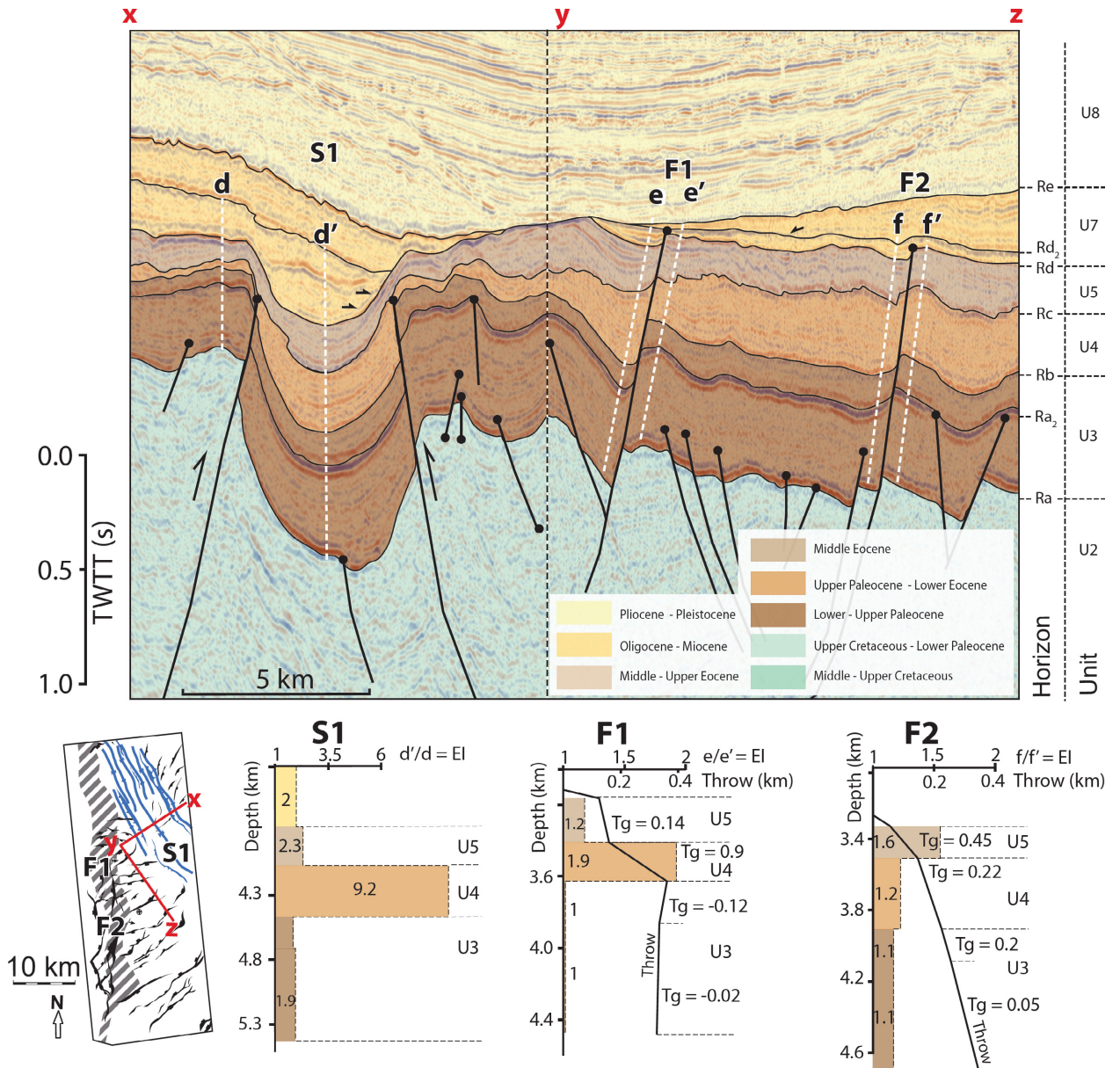


Fig. 7. Composite geosection from the southern survey across contractional domain (x-y) and extended domain (y-z) accompanied by throw vs. depth plots (including annotated throw gradients; Tg) and expansion indices displaying across fault stratigraphic thickness variations for fold (d'/d) and faults (e'/e and f'/f). Both the S1 syncline and the F1 and F2 normal faults show especially high expansion index values in the intervals covering upper Palaeocene to middle Eocene rocks. The high expansion index value in the Oligocene-Miocene interval is interpreted as post-kinematic infill of topography. Note that the geosection is shown in the time domain (S-TWTT), whereas the plots are depth converted.

and 1.2 (U4 at F1 and F2 respectively). F2 shows indications of hanging-wall expansion also in lower to upper Palaeocene strata (U3) with expansion index values of 1.1, whereas the same unit in F1 does not show any thickness variation across the fault. In the northern survey the upper Palaeocene to lower Eocene strata also display a marked hanging-wall expansion with expansion index values up to 2.8 (U4 & U5 at F4; Fig. 8).

Structures recording shortening

Structures attributed to shortening are orientated orthogonally (approximately 90°) to the strike of the normal faults described in Section 5.1 and include NW-SE striking synclines, thrust faults, and thrust propagation anticlines (Figs 5, 7, 8, 9 and 10). The strike of fold axes within both study areas are generally oriented NNW-SSE and are oriented oblique to the main strike of the

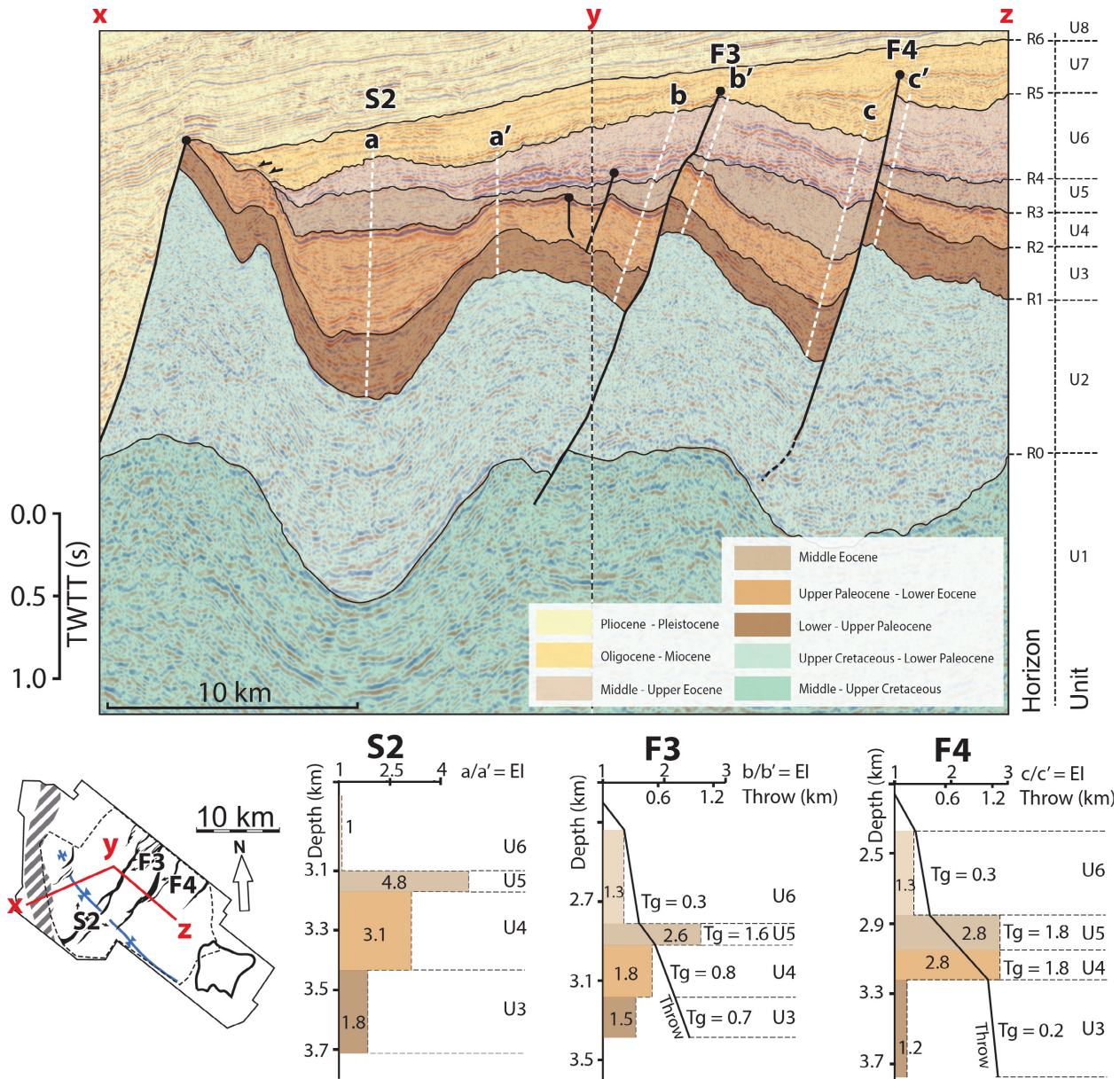


Fig. 8. Composite geosection from the southern survey across contractional domain (x-y) and extended domain (y-z) accompanied by throw vs. depth plots (including annotated throw gradients; Tg) and expansion indices displaying across fault stratigraphic thickness variations for fold (a/a') and faults (b/b' and c/c'). Both the S2 syncline and the F3 and F4 normal faults show especially high expansion index values in the intervals covering upper Palaeocene to middle Eocene rocks. F3 also indicate across fault hanging-wall thickening in the middle to upper Eocene interval. Note that the geosection is shown in the time domain (S-TWTT), whereas the plots are depth converted.

marginal high (19°–31°). The largest syncline (S1) in the southern survey is c. 25-km long along strike and c. 5.9-km wide with a maximum amplitude at horizon Rb of c. 797 ms (c. 980 m), whereas in the northern survey there is only one large syncline (S2) with a strike length of c. 45 km and a width of c. 8.4 km and a maximum amplitude of c. 855 ms (c. 1000 m) at horizon R2 (Figs 4 and 6). Thrusts and associated thrust propagation anticlines flank the synclines within the southern

survey study area and verge towards the syncline axis (Figs 7, 8, 9, and 10). In the southern survey there is a clustering of folds and thrusts in the middle part of the area as well as one cluster towards the NW corner as can be seen in Fig. 4.

A distinct observation is that all fold wavelengths and amplitudes are seen to increase along strike towards the marginal high (Fig. 10a–f). For S2 in the northern survey the amplitude and wavelength decrease away from the

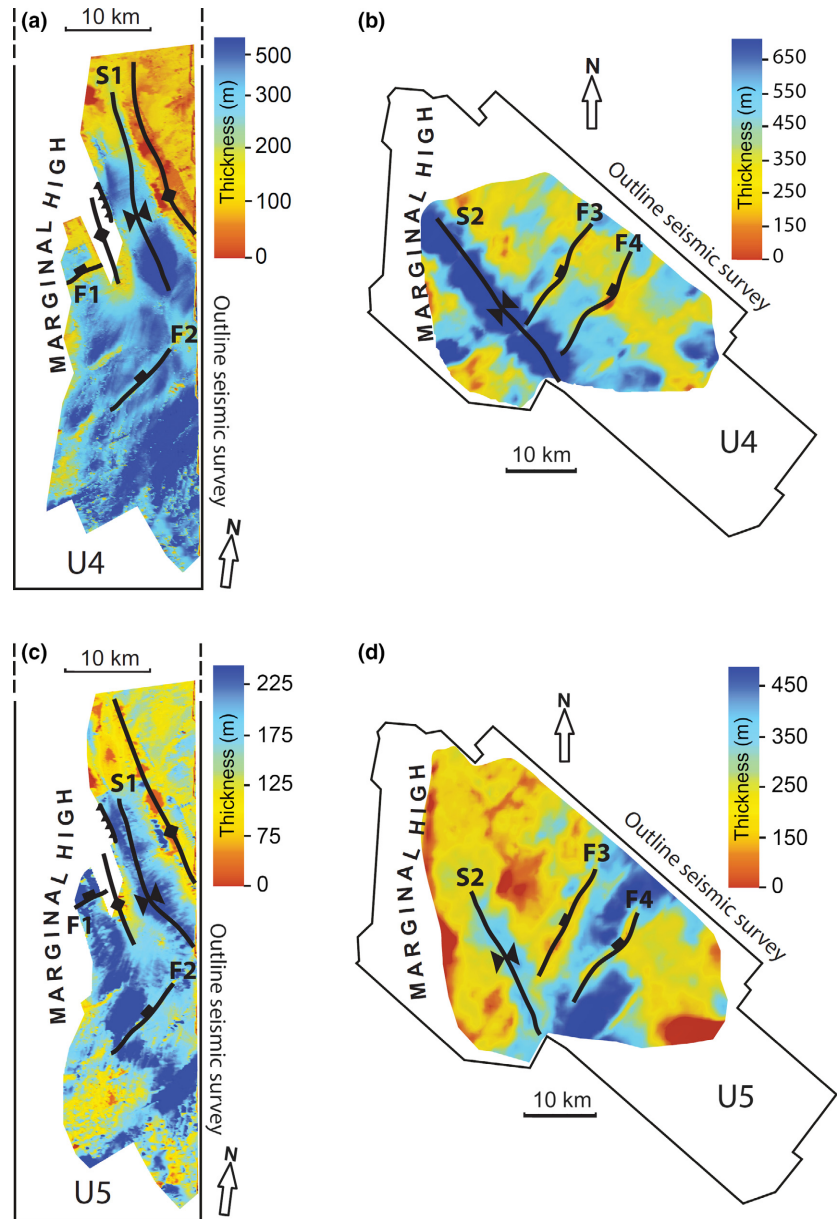


Fig. 9. Isochore thickness maps displaying thickness of seismic units U4 and U5 for the southern (a & c) and northern (b & d) surveys. The maps show true stratigraphic thickness and are based on depth-converted surfaces, the white parts represent areas where the seismic reflections could not be traced with high confidence (e.g. poor seismic quality, non-deposition or erosion).

marginal high can be seen in profile a-c in Fig. 10. In profile a, S2 has a wavelength along reflection R2 of c. 9 km, in profile b and c the wavelength increases to 10.5 km and 11.5 km respectively. Also here the amplitude of the folds decrease away from the marginal high with 405 ms (c. 470 m), 341 ms (c. 375 m) and 311 ms (c. 360 m) for reflection R2 at profile a, b and c respectively. S1 in the southern survey exhibits a trend that is similar to S2: the along-strike variation in wavelength is visualized in Fig. 10 where the syncline can be seen to widen along strike from profile d to f, i.e. when moving away from the marginal high. Profile d in Fig. 10 also displays an increase in thrust fault dip towards the marginal high accompanied by a decrease

in fold wavelengths, c. 4.6 km at Rb level, in contrast to profile e and f where the syncline has wavelengths of approximately 6.3 km and 7.2 km respectively. Profile d also covers the NW transition from S1 into an area with several folds, including an anticline that continues towards NW. The amplitude of the folds also decreases away from the marginal high with 716 ms (c. 1020 m) and 563 ms (c. 850 m) for reflection Rb at profile e and f respectively. For the southern survey the anticlines on the flanks of syncline S1 show a vergence towards the S1 axis (e.g. Fig. 5), and offset reflections can be observed in Figs 7 and 10. The magnitude of offset varies along strike of the anticlines (compare e.g. Fig. 10d, e).

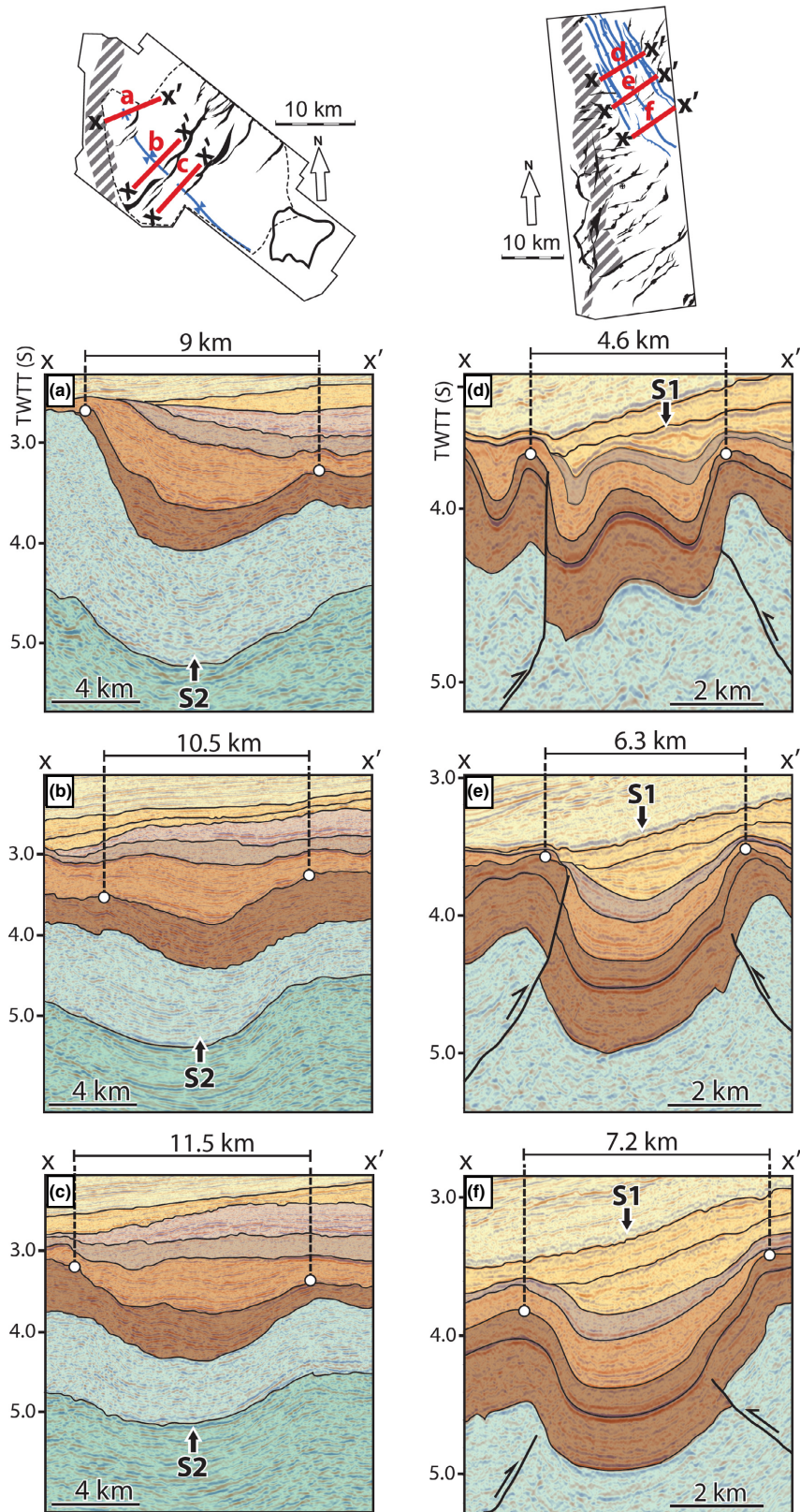


Fig. 10. Variations in fold geometry at location a–c along the northern survey S2 syncline and d–f along the southern survey S1 syncline, anticlines and thrusts. Note that fold wavelength and thrust dip increase towards the shear margin. Interval colours reflect the same division as in Fig. 3.

Stratigraphic thickness variations

The observed synclines in the study area are associated with a marked cross-fold increase in stratal thicknesses at certain structural levels and the synclines are associated with marked subsidence. This is evident in cross-sectional view (Figs 7 and 8), but particularly in time thickness maps (Fig. 9) where the most significant thickness maxima's are located along the axis of the synclines in the study area for the upper Palaeocene to Middle Eocene intervals (U4 and U5).

Variations in stratigraphic thickness observed between the shoulders of synclines and the synclinal axis are recorded and expressed as expansion indices (Figs 7 and 8). The expansion indices for S1 (Fig. 7) reveal that the lower Palaeocene to middle Eocene units (U3 to U7) all exhibit thickening towards the syncline axis. Note that we choose to record EI between the central part of the syncline and the NE-limb in both S1 and S2 because the SW-limbs are subjected to greater uplift and hence are partly eroded in places. The lower Palaeocene to middle Eocene units U3 to U5 display wedging geometries with parallel reflections that thin towards the syncline fold. Internal stratigraphic geometries of the lower part of the Oligocene-Miocene unit (U7) in the southern survey reveal that this unit is in fact on-lapping the underlying unit (Fig. 7). This infers that although U7 exhibits thickening towards the syncline axis in the southern survey, this thickening must be attributed to post-kinematic infill of an existing depocentre rather than syn-kinematic deposition. A maximum expansion index of 9.2 in the upper Palaeocene to lower Eocene (U4) is markedly higher than the relatively lower expansion index values for the lower to upper Palaeocene unit (U3; 1.9) and the middle Eocene unit (U5; 2.3) (Fig. 7). A similar thickening trend is seen for syncline S2 in the northern survey, where the lower Palaeocene to middle Eocene units (U3, U4 and U5) in S2 show a positive EI (Figs 8 and 9). S2 shows a continuous upward increase in expansion index values from 1.8 for the lower to upper Palaeocene unit (U3) via 3.1 for the upper Palaeocene to middle Eocene unit (U4) to a maximum of 4.8 for the middle Eocene unit (U5). In summary, both major synclines are associated with stratal expansion of the lower Palaeocene to middle Eocene units, where the maximum expansion occurs in Upper Palaeocene to Lowermost Eocene in the southern survey and Middle Eocene in the northern survey (Figs 7 and 8).

TECTONOSTRATIGRAPHIC EVOLUTION OF THE STUDY AREA

Here we elucidate the structural evolution of the Sørvestsnaget Basin from uppermost Cretaceous to Miocene times, using the presented data and observations concerning structural geometries and styles, sedimentary

thickness variations (EI and isochore maps), vertical throw distribution trends (T-z plots) and the character and geometry of the studied seismic units. On the basis of these results we subdivide the evolution of the study area and structures into i) pre-kinematic, ii) syn-kinematic and iii) post-kinematic phases. We stress that pre-, syn- and post-kinematic as used here are relative to the growth of faults and folds structures in the Sørvestsnaget Basin in Early Cenozoic times, and that we do not include kinematic events that precede the 'pre-kinematic' event in this study (e.g. Gudlaugsson *et al.*, 1998; Doré *et al.*, 1999; Faleide *et al.*, 2008).

Pre-kinematic phase (U1–U2)

The Cretaceous to lower Palaeocene intervals (U1 and U2; Figs 7 and 8) display very few continuous reflections that can be used to quantify stratigraphic thickness variations across faults. The depth to these intervals probably affects the seismic resolution which obscures details regarding the tectonic activity. However, qualitatively there is no evidence to suggest thickening across faults or folds during this time interval. Thus, these intervals are interpreted to represent a pre-kinematic stage; this is supported by Faleide *et al.* (1993a,b) that interpreted the basin to be characterized generally by regional subsidence in Middle Cretaceous following the Middle/Late Jurassic - Early Cretaceous rift event.

Syn-kinematic phase (U3–U6)

High expansion index values are recorded in the lower Palaeocene to Upper Eocene intervals (max expansion index 9.2 at S1 in unit U4 for the southern survey; Fig. 7), which together with high throw gradients (see throw gradients "Tg" in Figs 7 and 8) indicate that these intervals represent a syn-kinematic stage of the basin evolution spanning Palaeocene to late Eocene times (U3 to U5 for the southern survey and U3 to U6 for the northern survey; Figs 7 and 8).

The lower Palaeocene to upper Palaeocene interval (U3; Figs 7 and 8) show expansion index values ranging from 1.8 to 1.9 for the synclines, whereas the faults record expansion index values from 1 to 1.5 and can be termed early syn-kinematic in relation to the much higher expansion index values that follows. The climax of the syn-kinematic phase is recorded with the highest expansion index values in the upper Palaeocene to lower Eocene in the southern survey (EI = 1.2–9.2 for U4; Fig. 7), whereas in the northern survey the climax is recorded in the Middle Eocene (EI = 2.6–4.8 for U5; Fig. 8). Figure 9 shows that the synclines in the study area are associated with the greatest syn-kinematic stratigraphic thickness (Units 4 & 5), however, for Unit 5 in the northern survey the hanging-wall of

F4 display the greatest stratigraphic thickness. The syn-kinematic climax is followed by a waning stage represented by lower expansion index values for the middle Eocene in the southern survey (EI = 1.2–2.3 for U5; Fig. 7) and the middle to upper Eocene in the northern survey (EI = 1.3–4.8 for U6; Fig. 8). High throw gradients (Tg = 0.8–1.8) in the upper Palaeocene to lower Eocene and the middle Eocene intervals coincide with the high expansion index values and are indicative of surface breaching growth faulting (F1 to F4; Figs 7 and 8) (*sensu* Cartwright *et al.*, 1998).

Post-kinematic phase (U7–U8)

The uppermost studied intervals include the uppermost Eocene to present (U6–U8; Figs 7 and 8). The Oligocene to Miocene interval (U7; Figs 7 and 8) is characterized by an overall wedge-shaped geometry, thickening away from the marginal high. In some areas the Oligocene to Miocene interval appear to be related to tectonic activity, exemplified in S1 where the lower part of the interval (U7; Fig. 7) thickens in the syncline. However, onlapping reflections within the Oligocene to Miocene interval onto Rd and R5 are interpreted to reflect passive sedimentary infill of pre-existing topography rather than syn-kinematic sedimentation, thus indicating that these intervals are post-kinematic (Figs 7 and 8). In addition, at fault F4 the lowermost part of the Oligocene to Miocene interval (U7; Fig. 8) show internal geometries, hanging-wall thickening and a high throw gradient which indicates growth faulting and as such we attribute this to be reactivation of the fault possibly in Oligocene to Miocene times related to plate reorganization (e.g. Doré & Lundin, 1996; Ryseth *et al.*, 2003).

DISCUSSION

In the following discussion we aim to elucidate the timing and relationship between growth of folds and faults in the study area to shed new light on the understanding of the Southwestern Barents Shear Margin in general and the central and southern parts of the Sørvestsnaget especially.

Relative timing of shortening and extension in the study area

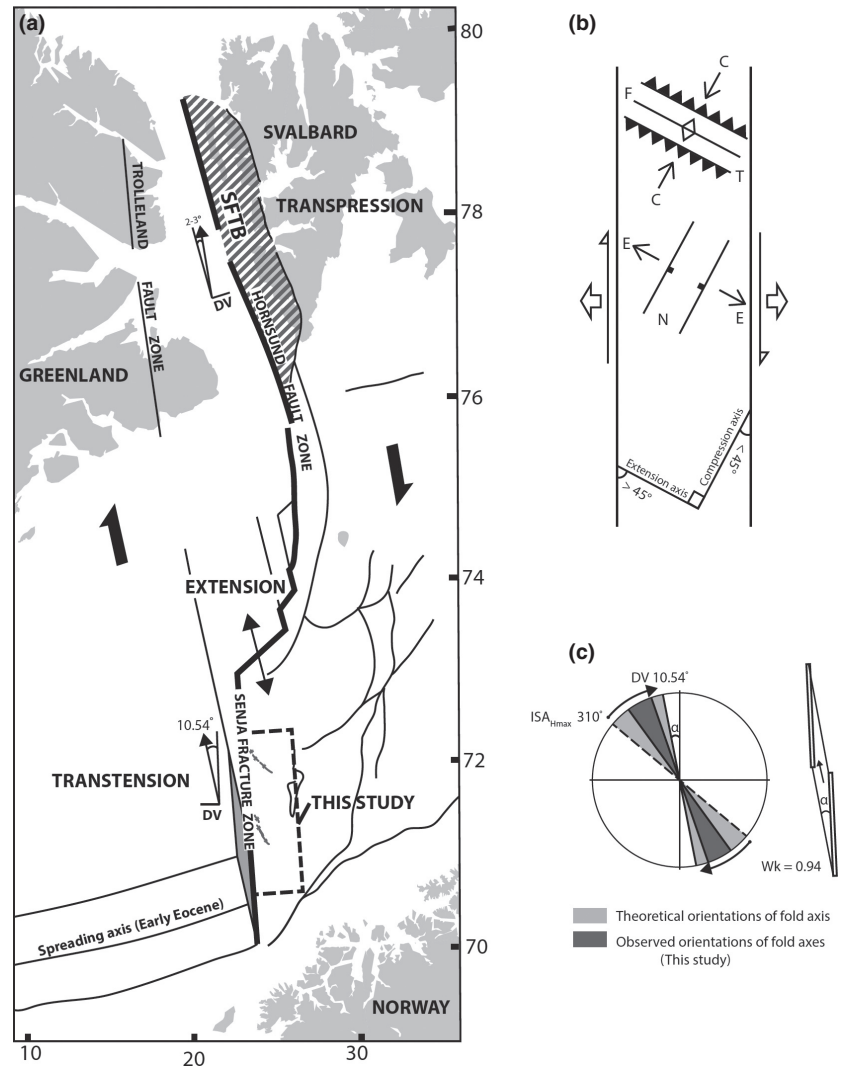
On the basis of the results and observations outlined in this paper, we interpret that NE-trending normal faults formed as a response to NW-directed extension, whereas NW-trending thrusts and folds are interpreted to have formed as a result of NE-directed shortening. We must therefore consider their relative timing: i) did extension and shortening occurred as separate phases of deformation or ii) did the two occur simultaneously?

Stratal thickening in normal fault hanging-wall and syncline depocentres within the study area forms a basis for discussing this spatio-temporal relationship. One possible hypothesis for the structuring described herein is that the structures formed in response to separate phases of extension and contraction. The analysis of expansion indices and time thickness maps indicates, however, that thrusting, folding and normal faulting took place largely simultaneous during deposition of lower Palaeocene to upper Eocene strata in the Sørvestsnaget Basin along the Senja Fracture Zone. Therefore, NE-directed shortening and NW-directed extension occurred largely coeval, and the observed structures did not form as a result of individual plate-scale pulses of contractional and extensional deformation (e.g. Figs 7, 8 and 9). We do not, however, exclude the possibility that there could be some temporal partitioning of deformation within the Eocene time interval, e.g. sub-seismic details of exactly when the faults or folding were active. Having established this synchronicity, there is still an outstanding question of what was the *driver* for coeval and orthogonal stretching and shortening; this will be addressed in following, where we discuss the role of regional tectonics and strain partitioning to explain the observed structures.

The opening of the Norwegian–Greenland Sea during the Eocene has been attributed to right lateral shear along the Senja Fracture Zone by several authors (e.g. Eldholm *et al.*, 1987; Faleide *et al.*, 1988, 1991, 1993a,b; Vågnes, 1997; Etc.), however, several authors have documented a minor transtensional component during opening based on obliquity between the COB and plate motion flowlines (Reksnes & Vågnes, 1985; Eldholm *et al.*, 1987; Faleide *et al.*, 1988). Reksnes & Vågnes (1985) reported that the initial opening occurred at a 10.54° angle to the Senja Fracture Zone (Breivik *et al.*, 1999) (Fig. 11a). The oblique shear angle decreased from 10.54° during initial opening at magnetic anomaly 24b to 7.78° at magnetic anomaly 13 (36 Ma) when the spreading ridge had travelled the majority of the length of the Senja Fracture zone (Vågnes, 1997). Vågnes (1997) estimated that the shear along the Senja margin lasted c. 21 Ma and that the mid oceanic ridge passed the shear margin at 71°57'N (just south of the northern survey) at chron A15 (c. 37 Ma). Although several studies suggest transtensional (as well as transpressional) components (e.g. Faleide *et al.*, 1993a; Gudlaugsson *et al.* 1998) along the Senja Shear Margin during this period, none of these studies address the possibility of coeval extension and shortening.

Folds can form during transtension due to horizontal contraction caused by the strike-slip component of deformation according to physical modelling results (Venkat-Ramani & Tikoff, 2002; Fig. 11b) and strain modelling (Fossen *et al.*, 2013). Using the relationship between the angle of divergence (divergence vector) and the kinematic vorticity number (W_k) which describes the relative

Fig. 11. (a) Redrawn map after Faleide *et al.* (1988) showing the opening angles (DV = divergence vector) and the relationship between the transpression along Western Svalbard, Extension in the 'pull-apart' basin in Vestbakken and northern Sorvestsnaget and the transtension along the Senja Fracture Zone. Thick black arrows illustrate the orientation of plate motion. (b) Model for initial orientation of extensional (E) and compressional (C) axis during transtension (redrawn after Sanderson & Marchini, 1984). Full and half arrows on the sides of the model illustrate the components of pure and simple shear in transtension respectively. F = fold, T = thrusts, N = normal faults. (c) Observed orientations of fold axis relative to expected range of fold axis from formation along ISA_{Hmax} (based on Fossen *et al.*, 2013) and rotation towards parallelism with the opening direction relative to the Senja Fracture Zone.



amount of simple vs. pure shear (Fossen *et al.*, 2013), we find that the initial opening along the Senja Fracture Zone has a Wk of c. 0.94 which would facilitate transtensional folding with axial planes oriented parallel to a maximum horizontal Instantaneous Stretching Axis (ISA_{Hmax}) orientation of c. 50° to the Senja Fracture Zone (Fig. 11c). In the two studied 3D datasets the general orientation of NW-SE trending contractional structures (folds e.g. S1 and S2 and reverse faults) is oriented at a c. 19°–36° angle relative to the Senja Fracture Zone (Fig. 9) suggesting that some rotation must have taken place after formation. Rotation of extension parallel fold axes during transtensional deformation have also been suggested in other basins such as the Devonian basins of western Norway where Osmundsen & Andersen (2001) suggested an anti-clockwise rotation of the regional syndepositional strain field. Venkat-Ramani & Tikoff (2002) showed in their physical models that transtensional fold-hinges rotate towards parallelism with the oblique movement direction, different from simple shear and transpression where the

hinges rotate towards parallelism with the shear-zone boundary. The orientation of folds recorded in this study fall well within the spectrum of orientations expected by such models. However, they are oriented at a greater angle (19°–36°) than the oblique plate movement recorded during the Eocene opening; 10.54°–7.78° from opening at magnetic anomaly 24b to plate reorganization and divergence at magnetic anomaly 13 (table 2 in Breivik *et al.*, 1999) (Fig. 11c). The difference between theoretical and observed orientations may indicate that the strain in the study area was not high enough to rotate the folds into parallelism with the oblique opening angle. The effect of strain accommodation and rotation of fold axes may also be supported by the observation that there is a greater rotation in the northern part (36°–19° from U4–U5) than in the southern part (29°–25° from Ud–Ue). This suggests that basin deformation and strain accumulation had a longer duration in the northern survey than in the southern survey, which fits well with the understanding of Greenland sliding along the Senja Fracture zone,

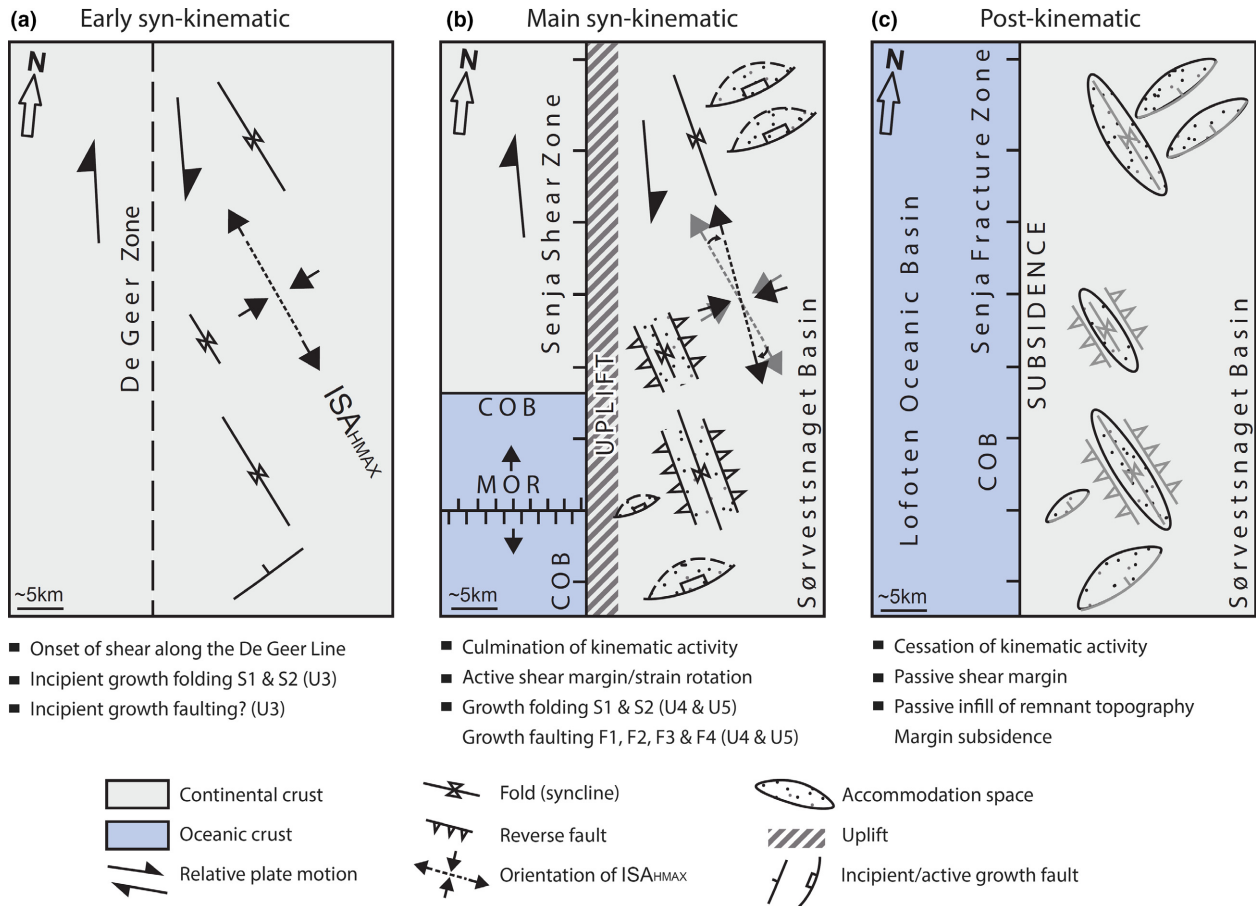


Fig. 12. Schematic illustration showing the three stages of kinematic activity resolved in this study; (a) Incipient growth folding recorded in Syncline S1 and S2 (U3) as well as possible incipient growth faulting at U3; (b) The main syn-kinematic period where fault and fold growth is most active and associated rotation of strain axis; (c) Cessation of fault and fold activity indicate establishment of a passive shear margin and passive sedimentary infill to remnant topography.

giving higher strain accumulation further north along the SFZ.

Folds with orientations such as in this study (ranging from 19 to 36° relative to the shear zones) could also form in a *transpressional* setting and could be a result of local transpression, perhaps due to irregularities, e.g. a restraining bend, along the margin (e.g. Sylvester, 1988), even though the margin on a regional scale is considered to be straight in map view. The observed orientations of the fold axial planes alone do not indicate transtension and have to be combined with the existing observations that indicate a transtensional component during the opening in the Eocene (e.g. Reksnes & Vågnes, 1985; Eldholm *et al.*, 1987). However, Fossen *et al.* (2013) indicate that one may also expect a pronounced hinge-parallel stretching component during transtensional folding which is accommodated by normal faulting. S1 in this study is associated with a normal fault in the middle of the syncline (e.g. Fig. 4) and S2 appear to be dissected by numerous normal faults along its entire length (e.g. Fig. 6) and as such show strong indications of hinge-

parallel stretching. Sanderson & Marchini (1984) also concluded that transtension may produce folds and thrusts at a high angle and extensional structures at a low angle to the shear zone, leading to crustal thinning, subsidence and basin development, similar to the results presented herein.

Combining the orientation of observed folds and normal faults as well as indications of hinge-parallel stretching (this study) with the oblique spreading direction (Reksnes & Vågnes, 1985; Eldholm *et al.*, 1987) we favour the interpretation that the deformation in the southern Sørvestsnaget Basin along the Senja Fracture Zone during the Eocene opening was mainly by partitioning of strain into shortening and extension by simple shear dominated transtension along a right lateral oblique shear margin.

Regional implications

As established above, we demonstrate that basin formation during the Palaeocene–Eocene opening of the

southern part of the Sørvestsnaget Basin concur with the overall understanding of the plate tectonic setting at this time. The De Geer Zone (e.g. Faleide *et al.*, 1993a) was a prerequisite for the oblique shear margin that caused transtensional strain partitioned into coeval contractional and extensional structures (Fig. 12a). The transtensional shear along the Southwestern Barents Sea Margin facilitated growth and rotation of folds, thrusts and normal faults during the upper Palaeocene to middle Eocene climax (Fig. 12b), followed by cessation of kinematic activity and passive infill of remnant topography (Fig. 12c). However, the Sørvestsnaget Basin has previously been treated mainly as a pull-apart basin controlled by normal faults (e.g. Ryseth *et al.*, 2003). In addition, salt diapirs attributed to passive rise during extension has been documented in the area (e.g. using the same dataset, northern survey; Perez-Garcia *et al.*, 2013). On the basis of the observations of strain partitioning and orientation of structures in this study, we suggest that the southern and margin-proximal part of the Sørvestsnaget Basin was controlled dominantly by the oblique shear movements along the Senja Shear Margin rather than the extension associated with the pull-apart basin formation in the northern parts of the basin.

The salt diapir located within the northern survey (e.g. Knutsen & Larsen, 1997; Perez-Garcia *et al.*, 2013) is the only documented and observed salt structure within the study area; however, with potential new and better resolution seismic reflection data in the future it can be resolved if and potentially if and how salt has affected the formation of faults, folds and thrusts documented in this study.

Partitioning of strain into contractional and extensional structures provides a basis to discuss structural complexities associated with basins and highs along the Western Barents Sea margin. Many contractional structures belonging to the Cenozoic syn- to post-rift period along the western Barents Sea margin are reported in the literature (e.g. the Veslemøy High and Senja Ridge; Doré & Lundin, 1996) and are often attributed to a pulse of inversion. This is also the case for structures in other areas along the NE Atlantic margin such as the Ormen Lange and Helland Hansen Arch in the mid Norwegian Margin. Suggested interpretation for the formation of these structures range from ridge push after creation of an active spreading ridge to more far-field causes as compressional forces from the Alpine and Pyrenean tectonics (e.g. Doré & Lundin, 1996).

De Paola *et al.* (2005) stated that partitioned transtension should be considered as an alternative to explain 'inversion structures' previously attributed to local or regional crustal shortening events. Pulsed extension-inversion-extension models are commonly used to explain basin evolution in a variety of onshore and offshore environments. Local inversion explained by far-field effects of orogenic events should be considered in the light of strain

partitioning in transtensional deformation as a more elegant explanation for observed structural complexities (De Paola *et al.*, 2005). In strike-slip tectonic regimes such as existed along the western Barents Sea margin during the early Cenozoic it should be expected that contractional structures (folds, reverse faults etc.) may form due to strain partitioning either in a simple shear, transpressional or transtensional domain locally (e.g. this paper and Sanderson & Marchini, 1984). Such structuring was presented by Seiler *et al.* (2013) that showed how the Santa Rosa basin deformed by oblique-divergent shear during the Neogene oblique opening of the Gulf of California, which resulted in partitioning of strain between normal faulting on discrete fault zones and distributed constructional strain that was accommodated by folding of the rock volume. As such we impose a more complex relationship between observed geometries and kinematics than for inversion models. We suggest that partitioned contraction during transtension, simple shear or transpression should be considered as an alternative mechanism to wholesale inversion to explain contractional structures (head on 'inversion' structures) of the SW Barents Sea Margin (e.g. Gabrielsen *et al.*, 1997), especially those structures documented on scarce 2D data and poor well-control. If the contractional structures are poorly dated due to limited well-control they can easily be misinterpreted to coincide with the change in spreading direction associated with anomaly 13, instead of being formed under a simple shear or transpressional/transtensional strain like the compressional structures of the Sørvestsnaget Basin.

SUMMARY AND CONCLUSIONS

Our analysis of the structural evolution in the southern Sørvestsnaget Basin during the Cenozoic opening of the Northern North Atlantic gives new insights into basin evolution during oblique shear. Our results show that during the late Palaeocene and early Eocene transtensional shear along the Southwestern Barents Sea Margin strain was partitioned and accommodated by coeval normal faults, folds and thrust faults in the Sørvestsnaget Basin. On the basis of this, we draw the following conclusions on basin deformation in shear margin basins:

- Deformation in basins located along sheared margins with a transtensional component can be expected to be characterized by formation of coeval extensional and contractional structures due to partitioning of strain.
- The orientation of structures is predictable with contractional and extensional structures oriented at a high angle to each other. The orientation of the structures is dependent on the direction of plate movement relative to the orientation of the shear margin.

- Transtensional folding and strain partitioning may explain contractional structures previously interpreted to be caused by separate pulses of compression/inversion.

Our results shed new light on timing and origin of contractional structures along the SW Barents Margin, and should facilitate constraints on timing of trap formation as well as provide a basin topography backdrop for prediction of reservoir (and seal) distribution. Accordingly it provides learnings applicable for petroleum exploration along transtensional margins in general, and specifically for the SW part of the Western Barents Margin which is located in a region of active exploration.

ACKNOWLEDGEMENTS

Shell Norway is acknowledged for providing data-access and funds for this study. Schlumberger is thanked for providing the University of Bergen with licenses for the Petrel software package, allowing in-house seismic interpretation. Permission to publish data from the TRIII-08 seismic survey as well as 2D seismic lines for geosection in Fig. 1 was granted by TGS. Diskos and Statoil are acknowledged for providing the NH9803 seismic survey. Constructive and insightful comments from Johan S. Claringbould, David Sanderson, Per Terje Osmundsen as well as editor Rebecca Bell have led to significant improvements of the final version of this paper.

CONFLICT OF INTEREST

No conflict of interest declared.

SUPPORTING INFORMATION

Additional Supporting Information may be found in the online version of this article:

- Figure S1. Uninterpreted seismic sections from Fig. 2.
- Figure S2. Uninterpreted seismic sections from Fig. 7.
- Figure S3. Uninterpreted seismic sections from Fig. 8.
- Figure S4. Uninterpreted seismic sections from Fig. 10.

REFERENCES

BADLEY, M.E., PRICE, J.D., DAHL, C.R. & AGDESTAIN, T. (1988) The structural evolution of the northern Viking Graben and its bearing upon extensional modes of basin formation. *J. Geol. Soc.*, **145**(3), 455–472.

BASILE, C. & BRUN, J.P. (1999) Transtensional faulting patterns ranging from pull-apart basins to transform continental margins: an experimental investigation. *J. Struct. Geol.*, **21**(1), 23–37.

BAUDON, C. & CARTWRIGHT, J. (2008a) Early stage evolution of growth faults: 3-D seismic insights from the Levant Basin, Eastern Mediterranean. *J. Struct. Geol.*, **30**(7), 888–898.

BAUDON, C. & CARTWRIGHT, J. (2008b) The kinematics of reactivation of normal faults using high resolution throw mapping. *J. Struct. Geol.*, **30**(8), 1072–1084.

BAUDON, C. & CARTWRIGHT, J.A. (2008c) 3-D seismic characterisation of an array of blind normal faults in the Levant Basin, Eastern Mediterranean. *J. Struct. Geol.*, **30**(6), 746–760.

BELL, R.E., MCNEILL, L.C., BULL, J.M., HENSTOCK, T.J., COLLIER, R.E.L. & LEEDER, M.R. (2009) Fault architecture, basin structure and evolution of the Gulf of Corinth Rift, central Greece. *Basin Res.*, **21**(6), 824–855.

BIRD, D. (2001) Shear margins: continent-ocean transform and fracture zone boundaries. *Lead. Edge*, **20**(2), 150–159.

BOUROULLEC, R., CARTWRIGHT, J.A., JOHNSON, H.D., LANSIGU, C., QUÉMENER, J.-M. & SAVANIER, D. (2004) Syndepositional faulting in the Grès d'Annot Formation, SE France: high-resolution kinematic analysis and stratigraphic response to growth faulting. *Geol. Soc. Lond. Spec. Publ.*, **221**(1), 241–265.

BREIVIK, A.J., FALEIDE, J.I. & GUDLAUGSSON, S.T. (1998) South-western Barents Sea margin: late Mesozoic sedimentary basins and crustal extension. *Tectonophysics*, **293**(1), 21–44.

BREIVIK, A.J., VERHOEF, J. & FALEIDE, J.I. (1999) Effect of thermal contrasts on gravity modeling at passive margins: results from the western Barents Sea. *J. Geophys. Res. Solid Earth*, **104**(B7), 15293–15311.

CARTWRIGHT, J., BOUROULLEC, R., JAMES, D. & JOHNSON, H. (1998) Polycyclic motion history of some Gulf Coast growth faults from high-resolution displacement analysis. *Geology*, **26**(9), 819–822.

CHILDS, C., WATTERSON, J. & WALSH, J.J. (1995) Fault overlap zones within developing normal fault systems. *J. Geol. Soc.*, **152**(3), 535–549.

CHILDS, C., NICOL, A., WALSH, J.J. & WATTERSON, J. (2003) The growth and propagation of synsedimentary faults. *J. Struct. Geol.*, **25**(4), 633–648.

CHRISTIE-BLICK, N. & BIDDLE, K.T. (1985) Deformation and basin formation along strike-slip faults. *SEPM Spec. Publ.*, **37**, 1–34.

CLEGG, P. & HOLDSWORTH, R.E. (2005) Complex deformation as a result of strain partitioning in transpression zones: an example from the Leinster Terrane, SE Ireland. *J. Geol. Soc.*, **162**(1), 187–202.

CLIFT, P.D., LORENZO, J., CARTER, A., HURFORD, A.J. & ODP LEG 159 Scientific Party (1997) Transform tectonics and thermal rejuvenation on the Côte d'Ivoire-Ghana margin, west Africa. *J. Geol. Soc.*, **154**(3), 483–489.

CORTI, G., Van WIJK, J., BONINI, M., SOKOUTIS, D., CLOETINGH, S., INNOCENTI, F. & MANETTI, P. (2003) Transition from continental break-up to punctiform seafloor spreading: how fast, symmetric and magmatic. *Geophys. Res. Lett.*, **30**(12).

De PAOLA, N., HOLDSWORTH, R.E., MCCAFFREY, K.J. & BARCHI, M.R. (2005) Partitioned transtension: an alternative to basin inversion models. *J. Struct. Geol.*, **27**(4), 607–625.

DEWEY, J.F., HOLDSWORTH, R.E. & STRACHAN, R.A. (1998) Transpression and transtension zones. *Geol. Soc. Lond. Spec. Publ.*, **135**(1), 1–14.

- DORÉ, A.G. (1991) The structural foundation and evolution of Mesozoic seaways between Europe and the Arctic. *Palaeogeogr. Palaeoclimatol. Palaeoecol.*, **87**(1–4), 441–492.
- DORÉ, A.G. & LUNDIN, E.R. (1996) Cenozoic compressional structures on the NE Atlantic margin; nature, origin and potential significance for hydrocarbon exploration. *Petrol. Geosci.*, **2**(4), 299–311.
- DORÉ, A.G., LUNDIN, E.R., JENSEN, L.N., BIRKELAND, Ø., ELIASSEN, P.E. & FICHLER, C. (1999) Principal tectonic events in the evolution of the northwest European Atlantic margin. In Geological society, London, petroleum geology conference series (Vol. 5, pp. 41–61). Geological Society of London.
- DORÉ, A.G., LUNDIN, E.R., GIBBONS, A., SÖMME, T.O. & TORUDBAKKEN, B.O. (2015) Transform margins of the Arctic: a synthesis and re-evaluation. *Geol. Soc. Lond. Spec. Publ.*, **431**, SP431–SP438.
- EBINGER, C.J. (1989) Geometric and kinematic development of border faults and accommodation zones, Kivu-Rusizi Rift, Africa. *Tectonics*, **8**(1), 117–133.
- ELDHOLM, O., FALEIDE, J.I. & MYHRE, A.M. (1987) Continent-ocean transition at the western Barents Sea/Svalbard continental margin. *Geology*, **15**(12), 1118–1122.
- ELDHOLM, O., TSIKALAS, F. & FALEIDE, J.I. (2002) Continental margin off Norway 62–75° N: Palaeogene tectono-magmatic segmentation and sedimentation. *Geol. Soc. Lond. Spec. Publ.*, **197**(1), 39–68.
- FALEIDE, J.I., BJØRLYKKE, K. & GABRIELSEN, R.H. (2010) Geology of the norwegian continental shelf. *Petroleum Geoscience*, pp. 467–499. Springer, Berlin.
- FALEIDE, J.I., GUDLAUGSSON, S.T. & JACQUART, G. (1984) Evolution of the western Barents Sea. *Mar. Pet. Geol.*, **1**(2).
- FALEIDE, J.I., MYHRE, A.M. & ELDHOLM, O. (1988) Early Tertiary volcanism at the western Barents Sea margin. *Geol. Soc. Lond. Spec. Publ.*, **39**(1), 135–146.
- FALEIDE, J.I., GUDLAUGSSON, S.T., ELDHOLM, O., MYHRE, A.M. & JACKSON, H.R. (1991) Deep seismic transects across the sheared western Barents Sea-Svalbard continental margin. *Tectonophysics*, **189**(1), 73–89.
- FALEIDE, J.I., VÅGNES, E. & GUDLAUGSSON, S.T. (1993a) Late Mesozoic-Cenozoic evolution of the south-western Barents Sea in a regional rift-shear tectonic setting. *Mar. Pet. Geol.*, **10**(3), 186–214.
- FALEIDE, J.I., VÅGNES, E. & GUDLAUGSSON, S.T. (1993b) Late Mesozoic-Cenozoic evolution of the southwestern Barents Sea. In Geological Society, London, Petroleum Geology Conference series (Vol. 4, pp. 933–950). Geological Society of London.
- FALEIDE, J.I., SOLHEIM, A., FIEDLER, A., HJELSTUEN, B.O., ANDERSEN, E.S. & VANNESTE, K. (1996) Late Cenozoic evolution of the western Barents Sea-Svalbard continental margin. *Global Planet. Change*, **12**(1), 53–74.
- FALEIDE, J.I., TSIKALAS, F., BREIVIK, A.J., MJELDE, R., RITZMANN, O., ENGEN, O., WILSON, J. & ELDHOLM, O. (2008) Structure and evolution of the continental margin off Norway and the Barents Sea. *Episodes*, **31**(1), 82–91.
- FOSSEN, H., TEYSSIER, C. & WHITNEY, D.L. (2013) Transtensional folding. *J. Struct. Geol.*, **56**, 89–102.
- GABRIELSEN, R.H. (1984) Long-lived fault zones and their influence on the tectonic development of the southwestern Barents Sea. *J. Geol. Soc.*, **141**(4), 651–662.
- GABRIELSEN, R.H., FÆRSETH, R.B., JENSEN, L.N., KALHEIM, J.E. & RIIS, F. (1990) Structural elements of the Norwegian continental shelf. Part I: the Barents Sea region. *Norm. Petrol. Direct. Bull.*, **6**, 1–33.
- GABRIELSEN, R.H., GRUNNALEITE, I. & RASMUSSEN, E. (1997) Cretaceous and tertiary inversion in the Bjørnøyrenna Fault Complex, south-western Barents Sea. *Mar. Pet. Geol.*, **14**, 165–178.
- GIBA, M., WALSH, J.J. & NICOL, A. (2012) Segmentation and growth of an obliquely reactivated normal fault. *J. Struct. Geol.*, **39**, 253–267.
- GUDLAUGSSON, S.T., FALEIDE, J.I., JOHANSEN, S.E. & BREIVIK, A.J. (1998) Late Palaeozoic structural development of the south-western Barents Sea. *Mar. Pet. Geol.*, **15**(1), 73–102.
- HIGGINS, S., CLARKE, B., DAVIES, R.J. & CARTWRIGHT, J. (2009) Internal geometry and growth history of a thrust-related anticline in a deep water fold belt. *J. Struct. Geol.*, **31**(12), 1597–1611.
- HOLDSWORTH, R.E., TAVARNELLI, E., CLEGG, P., PINHEIRO, R.V.L., JONES, R.R. & MCCAFFREY, K.J.W. (2002) Domainal deformation patterns and strain partitioning during transpression: an example from the Southern Uplands terrane, Scotland. *J. Geol. Soc.*, **159**(4), 401–415.
- HUGGINS, P., WATTERSON, J., WALSH, J.J. & CHILDS, C. (1995) Relay zone geometry and displacement transfer between normal faults recorded in coal-mine plans. *J. Struct. Geol.*, **17**, 1741–1755.
- HUISMANS, R.S., PODLADCHIKOV, Y.Y. & CLOETINGH, S.A.P.L. (2001) Dynamic modeling of the transition from passive to active rifting, application to the Pannonian basin. *Tectonics*, **20**(6), 1021–1039.
- JACKSON, C.A.L. & ROTEVATN, A. (2013) 3-D seismic analysis of the structure and evolution of a salt-influenced normal fault zone: a test of competing fault growth models. *J. Struct. Geol.*, **54**, 215–234.
- JACKSON, H.R., FALEIDE, J.I. & ELDHOLM, O. (1990) Crustal structure of the sheared southwestern Barents Sea continental margin. *Mar. Geol.*, **93**, 119–146.
- JACKSON, C.A.L., BELL, R., ROTEVATN, A. & TVEDT, A.B. (2017) Techniques to determine the kinematics of synsedimentary normal faults and implications for fault growth models. *Geol. Soc. Lond. Spec. Publ.*, **439**, SP439–22. ISO 690.
- JONES, R.R., HOLDSWORTH, R.E., CLEGG, P., MCCAFFREY, K. & TAVARNELLI, E. (2004) Inclined transpression. *J. Struct. Geol.*, **26**(8), 1531–1548.
- KEAREY, P. & VINE, F.J. (1996) *Global Tectonics*, 2nd edn. 333 pp. Blackwell, New York, NY.
- KNUTSEN, S.M. & LARSEN, K.I. (1997) The late Mesozoic and Cenozoic evolution of the Sørvestsnaget Basin: a tectonostratigraphic mirror for regional events along the Southwestern Barents Sea margin? *Mar. Pet. Geol.*, **14**(1), 27–54.
- LEEVEY, K.A., GABRIELSEN, R.H., FALEIDE, J.I. & BRAATHEN, A. (2011) A transpressional origin for the West Spitsbergen fold-and-thrust belt: insight from analog modeling. *Tectonics*, **30**(2).
- LEHNER, P. & De RUITER, P.A.C. (1977) Structural history of Atlantic margin of Africa. *AAPG Bull.*, **61**(7), 961–981.

- LORENZO, J.M. (1997) Sheared continent–ocean margins: an overview. *Geo-Mar. Lett.*, **17**(1), 1–3.
- MANSFIELD, C.S. & CARTWRIGHT, J.A. (1996) High resolution fault displacement mapping from three-dimensional seismic data: evidence for dip linkage during fault growth. *J. Struct. Geol.*, **18**(2), 249–263.
- MCCLAY, K.R., DOOLEY, T., WHITEHOUSE, P. & MILLS, M. (2002) 4-D evolution of rift systems: Insights from scaled physical models. *AAPG Bull.*, **86**(6), 935–960.
- MJELDE, R., BREIVIK, J.A., ELSTAD, H., RYSETH, A.E., SKILBREI, J.G.O., SHIMAMURA, H., MURAI, Y. & NISHIMURA, Y. (2002) Geological development of the Sørvestsnaget Basin, SW Barents Sea, from ocean bottom seismic, surface seismic and potential field data. *Nor. Geol. Tidsskr.*, **82**, 183–202.
- MOUNT, V.S. & SUPPE, J. (1987) State of stress near the San Andreas fault: implications for wrench tectonics. *Geology*, **15**(12), 1143–1146. Vol. 82, pp. 183–202.
- MOUSTAFA, A.R. (1993) Structural characteristics and tectonic evolution of the east-margin blocks of the Suez rift. *Tectonophysics*, **223**(3–4), 381–399.
- MYHRE, A.M., ELDHOLM, O. & SUNDVOR, E. (1982) The margin between Senja and Spitsbergen fracture zones: implications from plate tectonics. *Tectonophysics*, **89**(1), 33–50.
- NALIBOFF, J. & BUTTER, S.J. (2015) Rift reactivation and migration during multiphase extension. *Earth Planet. Sci. Lett.*, **421**, 58–67.
- NICOL, A., WATTERSON, J., WALSH, J.J. & CHILDS, C. (1996) The shapes, major axis orientations and displacement patterns of fault surfaces. *J. Struct. Geol.*, **18**(2), 235–248.
- NOTTVEDT, A., BERGLUND, L.T., RASMUSSEN, E. & STEEL, R.J. (1988) Some aspects of Tertiary tectonics and sedimentation along the western Barents Shelf. *Geol. Soc. Lond. Spec. Publ.*, **39**(1), 421–425.
- OLDOW, J.S. (2003) Active transtensional boundary zone between the western Great Basin and Sierra Nevada block, western US Cordillera. *Geology*, **31**(12), 1033–1036.
- OSMUNDSEN, P.T. & ANDERSEN, T.B. (2001) The middle Devonian basins of western Norway: sedimentary response to large-scale transtensional tectonics? *Tectonophysics*, **332**, 51–68.
- PEREZ-GARCIA, C., SAFRONOVA, P.A., MIENERT, J., BERNDT, C. & ANDREASSEN, K. (2013) Extensional rise and fall of a salt diapir in the Sørvestsnaget Basin, SW Barents Sea. *Mar. Pet. Geol.*, **46**, 129–143.
- PETERSEN, K., CLAUSEN, O. & KORSTGÅRD, J. (1992) Evolution of a salt-related listric growth fault near the D-1 well, block 5605, Danish North Sea: displacement history and salt kinematics. *J. Struct. Geol.*, **14**, 565–577.
- RAVNÅS, R. & STEEL, R.J. (1997) Contrasting styles of Late Jurassic syn-rift turbidite sedimentation: a comparative study of the Magnus and Oseberg areas, northern North Sea. *Mar. Pet. Geol.*, **14**(4), 417–449.
- REKSNES, P.A. & VÅGNES, E. (1985) Evolution of the Greenland Sea and Eurasia basin. Cand. Scient. Thesis. University of Oslo, Oslo.
- RITZMANN, O. & FALEIDE, J.I. (2007) Caledonian basement of the western Barents Sea. *Tectonics*, **26**(5).
- RYKKELID, E. & FOSSEN, H. (2002) Layer rotation around vertical fault overlap zones: observations from seismic data, field examples, and physical experiments. *Mar. Pet. Geol.*, **19**(2), 181–192.
- RYSETH, A., AUGUSTSON, J.H., CHARNOCK, M., HAUGERUD, O., KNUTSEN, S.-M., MIDBØE, P.S., OPPSAL, J.G. & SUNDSBØ, G. (2003) Cenozoic stratigraphy and evolution of the Sørvestsnaget Basin, southwestern Barents Sea. *Nor. J. Geol./Norsk Geologisk Forening*, **83**(2).
- SANDERSON, D.J. & MARCHINI, W.R.D. (1984) Transpression. *J. Struct. Geol.*, **6**(5), 449–458.
- SCRUTTON, R.A. (1979) On sheared passive continental margins. *Tectonophysics*, **59**(1), 293–305.
- SEILER, C., FLETCHER, J.M., QUIGLEY, M.C., GLEADOW, A.J. & KOHN, B.P. (2010) Neogene structural evolution of the Sierra San Felipe, Baja California: evidence for proto-gulf transtension in the Gulf Extensional Province? *Tectonophysics*, **488**(1), 87–109.
- SEILER, C., QUIGLEY, M.C., FLETCHER, J.M., PHILLIPS, D., GLEADOW, A.J.W. & KOHN, B.P. (2013) Stratigraphy and ⁴⁰Ar/³⁹Ar geochronology of the Santa Rosa basin, Baja California: dynamic evolution of a constrictional rift basin during oblique extension in the Gulf of California. *Basin Res.*, **25**, 388–418.
- SHARP, I.R., GAWTHORPE, R.L., UNDERHILL, J.R. & GUPTA, S. (2000) Fault-propagation folding in extensional settings: examples of structural style and synrift sedimentary response from the Suez rift, Sinai, Egypt. *Geol. Soc. Am. Bull.*, **112**(12), 1877–1899.
- SPATHOPOULOS, F. (1996) An insight on salt tectonics in the Angola Basin, South Atlantic. *Geol. Soc. Lond. Spec. Publ.*, **100**(1), 153–174.
- STORTI, F. & POBLET, J. (1997) Growth stratal architectures associated to decollement folds and fault-propagation folds, Inferences on fold kinematics. *Tectonophysics*, **282**(1), 353–373.
- SUPPE, J., CHOU, G.T. & HOOK, S.C. (1992) Rates of folding and faulting determined from growth strata. In: *Thrust Tectonics* (Ed. by K.R. McClay), pp. 105–121. Chapman and Hall, New York.
- SYLVESTER, A.G. (1988) Strike-slip faults. *Geol. Soc. Am. Bull.*, **100**(11), 1666–1703.
- TALWANI, M. & ELDHOLM, O. (1977) Evolution of the Norwegian–Greenland sea. *Geol. Soc. Am. Bull.*, **88**(7), 969–999.
- THORSEN, C.E. (1963) Age of growth faulting in southeast Louisiana. *Gulf Coast Assoc. Geol. Soc. Trans.*, **13**, 103–110.
- TSIKALAS, F., FALEIDE, J.I. & ELDHOLM, O. (2001) Lateral variations in tectono-magmatic style along the Lofoten–Vesterålen volcanic margin off Norway. *Mar. Pet. Geol.*, **18**(7), 807–832.
- TSIKALAS, F., ELDHOLM, O. & FALEIDE, J.I. (2002) Early Eocene sea floor spreading and continent–ocean boundary between Jan Mayen and Senja fracture zones in the Norwegian–Greenland Sea. *Mar. Geophys. Res.*, **23**(3), 247–270.
- TVEDT, A.B.M., ROTEVATN, A., JACKSON, C.A.L., FOSSEN, H. & GAWTHORPE, R.L. (2013) Growth of normal faults in multi-layer sequences: a 3-D seismic case study from the Egersund Basin, Norwegian North Sea. *J. Struct. Geol.*, **55**, 1–20.
- TVEDT, A.B., ROTEVATN, A. & JACKSON, C.A. (2016) Supra-salt normal fault growth during the rise and fall of a diapir: perspectives from 3D seismic reflection data, Norwegian North Sea. *J. Struct. Geol.*, **91**, 1–26.

- VÄGENES, E. (1997) Uplift at thermo-mechanically coupled ocean–continent transforms: modeled at the Senja fracture zone, southwestern Barents Sea. *Geo-Mar. Lett.*, **17**(1), 100–109.
- VENKAT-RAMANI, M. & TIKOFF, B. (2002) Physical models of transtensional folding. *Geology*, **30**(6), 523–526.
- WALSH, J.J., NICOL, A. & CHILDS, C. (2002) An alternative model for the growth of faults. *J. Struct. Geol.*, **24**(11), 1669–1675.
- WALSH, J.J., BAILEY, W.R., CHILDS, C., NICOL, A. & BONSON, C.G. (2003) Formation of segmented normal faults: a 3-D perspective. *J. Struct. Geol.*, **25**(8), 1251–1262.
- WILSON, P., ELLIOTT, G.M., GAWTHORPE, R.L., JACKSON, C.A.L., MICHELSEN, L. & SHARP, I.R. (2013) Geometry and segmentation of an evaporite–detached normal fault array: 3D seismic analysis of the southern Bremstein Fault Complex, offshore mid-Norway. *J. Struct. Geol.*, **51**, 74–91.
- WITHJACK, M.O., SCHLISCHE, R.W. & OLSEN, P.E. (1998) Diachronous rifting, drifting, and inversion on the passive margin of central eastern North America: an analog for other passive margins. *AAPG Bull.*, **82**(5), 817–835.
- ZIEGLER, P.A. (1992) North Sea rift system. *Tectonophysics*, **208**(1), 55–75.

Manuscript received 1 March 2017; In revised form 22 May 2017; Manuscript accepted 5 July 2017.